ISSN 0280-5316
ISRN LUTFD2/TFRT--5909--SE

Wind Speed Prediction Models and Their Use in Wind Turbine Control

Paolo Mattachini

Lund University
Department of Automatic Control
January 2013

Lund University
Department of Automatic Control
Box 118
SE-221 00 Lund Sweden

Document name
MASTER THESIS

Date of issue
January 2013

Document Number
ISRN LUTFD2/TFRT--5909--SE

Author(s)
Paolo Mattachini

Supervisor
Daria Madjidian, Dept. of Automatic Control, Lund University, Sweden
Anders Rantzer, Dept. of Automatic Control, Lund University, Sweden (examiner)

Sponsoring organization

Title and subtitle
Wind speed prediction models and their use in wind turbine control

Abstract
Wind energy production is a section that became bigger and bigger thanks to the interests in finding new ways to produce energy that do not involve fossil fuels because of environment concerns, because of their costs and because of their limited amount. Even though wind energy was exploited also in the past, for example in wind mills, it is with wind turbines that all the problems affecting these systems started to be taken into account and to be studied deeply. Rising sizes, flexible materials used, aerodynamics, unfriendly environments, wind variability are some of the challenges to face in order to improve efficiency and extend the life and reliability of these systems. It is in this wide and various context that wind prediction models are needed to understand and to know in advance, in a wind farm, how wind will change and which effects it will have on a turbine and the following ones. In this work an approach to forecast the wind at downwind positions, using upwind turbines as sensors, is proposed. The work is based on real data from Thanet Wind Farm provided by Vestas Wind Systems A/S. The models found are relevant only for the sequences taken into account but they show the possibility to exploit existing turbines as wind sensors and open the way for further development of this work. This argument appear to be (to my knowledge) new, since in literature almost no references were found.

Keywords

Classification system and/ or index terms (if any)

Supplementary bibliographical information

ISSN and key title
0280-5316

ISBN

Language
English

Number of pages
1-94

Recipient's notes

Security classification

To my family.

Acknowledgments

First of all I would like to thank Professor Bittanti, who gave me the possibility to work on my thesis abroad and to Professor Rantzer who welcomed me in Lund and managed to find this very interesting subject. A heartfelt thank you is needed also for PhD student Daria Madjidian, for all the hours he spent supervising my work and for his valuable suggestions. To all my friends also, who never stopped supporting me and to Rebecca, who always managed to encourage me and always believed in me. Finally the most special thank you goes to my family, for all the effort and support they put in these years.

Contents

List of Figures

List of Tables

Prefazione

Il settore dell'energia eolica è diventato sempre più grande grazie all'interesse a trovare nuovi modi di produrre energia che fossero svincolati dai combustibili fossili a causa di problemi ambientali, del costo delle materie prime e per la loro limitatezza. Sebbene l'energia eolica è stata sfruttata molto anche nel passato, per esempio nei mulini a vento, è tramite le turbine eoliche che tutti i problemi che affliggono questi sistemi sono stati presi in considerazione e studiati approfonditamente. Dimensioni crescenti, materiali flessibili, caratteristiche aerodinamiche, ambienti ostili e variabilità del vento sono solo alcune delle sfide da affrontare per migliorare l'efficienza e prolungare la vita e l'affidabilità di questi sistemi. Modelli di predizione sono necessari in un contesto così vario e ampio per capire e sapere in anticipo, in un parco eolico, come cambierà il vento e che effetti avrà su una turbina e sulle successive. In questo lavoro viene proposto un approccio per predire il vento in posizioni a valle di una turbina, sfruttando le misure della stessa che agisce quindi anche come sensore. Questo studio è basato su misure reali, provenienti dal parco eolico di Thanet e fornite dalla Società Vestas. I modelli trovati sono rilevanti solo per le sequenze di dati utilizzati ma mostrano la possibilità di sfruttare turbine esistenti come sensori del vento per le turbine a valle e aprono la strada per futuri sviluppi in questo senso. L'argomento trattato sembra essere innovativo in quanto in letteratura non sono stati trovati molti riferimenti a riguardo.

Parole chiave: velocità del vento effettiva, stima del vento, modelli di correlazione del vento, predizione del vento

Abstract

Wind energy production is a section that became bigger and bigger thanks to the interests in finding new ways to produce energy that do not involve fossil fuels because of environment concerns, because of their costs and because of their limited amount. Even though wind energy was exploited also in the past, for example in wind mills, it is with wind turbines that all the problems affecting these systems started to be taken into account and to be studied deeply. Rising sizes, flexible materials used, aerodynamics, unfriendly environments, wind variability are some of the challenges to face in order to improve efficiency and extend the life and reliability of these systems. It is in this wide and various context that wind prediction models are needed to understand and to know in advance, in a wind farm, how wind will change and which effects it will have on a turbine and the following ones. In this work an approach to forecast the wind at downwind positions, using upwind turbines as sensors, is proposed. The work is based on real data from Thanet Wind Farm provided by Vestas Wind Systems A/S. The models found are relevant only for the sequences taken into account but they show the possibility to exploit existing turbines as wind sensors and open the way for further development of this work. This argument appear to be (to my knowledge) new, since in literature almost no references were found.

Keywords: Effective wind speed, wind estimate, wind correlation models, wind prediction

Riassunto

Questo lavoro di tesi, nato grazie ad una collaborazione tra l'Università di Lund e la Società Vestas, mira ad indagare la possibile esistenza di correlazione tra misure di velocità del vento tra turbine in un parco eolico. L'intero studio è basato su misurazioni vere, provenienti da Thanet Wind Farm, in Inghilterra. Ricerche bibliografiche e successiva analisi dei dati hanno confermato che le misure del vento effettutate dagli anemometri delle turbine forniscono misure non affidabili, in quanto molto disturbate, rumorose e puntuali. Per superare questo problema

- è stato introdotto il concetto di *Effective Wind Speed*, riferimenti al quale sono disponibili in bibliografia;
- è stato implementato un metodo per stimare la suddetta quantità;
- sono state svolte simulazioni per la sua validazione tramite la definizione.

Successivamente è stata sviluppata un'ipotesi sul possibile modello del vento, giustificandola teoricamente. Tramite analisi di correlazione sono state individuate le sequenze di dati che mostrassero interazioni rilevanti e due metodi per stimare i modelli sono stati implementati e testati sui dati disponibili. In seguito i modelli ottenuti sono stati analizzati per effettuare eventuali semplificazioni e infine validati tramite differenti criteri. I risultati ottentui hanno confermato le iniziali ipotesi di modello del vento. E' quindi stato possibile calcolare un predittore a k passi in avanti che risulta fornire buoni risultati. Infine un nuovo semplice schema di controllo è stato implementato, mostrando i benefici che le previsioni avrebbero nel controllo.

Chapter 1

Introduction

Wind is recognized worldwide as an environmentally friendly solution to energy shortage. With the need of energy growing more and more over the years and because of the will to look for energetic solutions different from fossil fuels it has become an interesting area both of research and production. Wind energy is a fast-growing interdisciplinary field that encompasses many different branches of engineering and science[11]. The installed capacity of wind grew at an average rate of 29% per year over the years 2002-2007[12]. In spite of the very fast grow of wind energy installed capacity, engineering challenges still exist: in order to increase power capture of the wind turbines the rotor size grew bigger and bigger and because of the need of more constant winds also the height increased, since far from the ground the wind is more constant. Modern wind turbines are large, flexible structures operating in uncertain environments and lend themselves nicely to advanced control solutions[11].

1.1 Objectives of this work

In wind farms each turbine generates wakes which affects the wind field and can disturb the behavior of neighboring turbines. The goal of the work is to study the relationship between turbines manifested in the wind field and to use this relationship to explore the possibility to forecast wind speed in a certain place (x, y) inside a wind farm using upwind turbines as wind sensors. The location (x, y) for which is interesting to have a prediction of wind speed is, of course, a downwind turbine. If this problem can be solved it would mean to have less sensors on a turbine, decreasing the risk of faults and the cost of the device. Work towards this direction can be found in [8] and [16]. In these works it is concluded that informations from upwind turbines are not useful for predictions. Other earlier forecasting attempts referred in literature use data collected at the site under consideration. A classical time series analysis is used and leads to various Box -Jenkins $ARMA(p, q)$ models, where the p most recent wind-speeds

and the q most recent forecasting errors are used as inputs.[9] In [9] an artificial neural network, together with cross correlation in neighbouring sites is used to forecast wind speed up to several hours. Another approach proposed in [10] uses artificial neural network models for forecasting average values of 10 minutes or 1 hour using as inputs wind speed and their derivatives. In [15] instead it is assumed that the effective wind speed can be a better measurement to use for prediction. Results seem promising. It is according to this work that this research has been carried out. Furthermore the solution to this problem could have direct influences on energy production since it would permit to know in advance which actions should be performed by the controller in order to better fulfill its duties.

1.2 Main Contributions

The contributions that this work should be able to offer can be resumed in the following:

- development of a method to identify wind speed models between turbines using the concept of *Effective Wind Speed*;
- it shows which identification approaches give better results, paving the way for further developments of the methodology;
- through simulation it shows the benefits of prediction in control also in this case opening the way for further research in the field.

1.3 Chapter Organization

The work is organized in the following way:

- **Chapter 2** is a quick introduction to the wind: it describes what the wind is, the power available and the solutions adopted to exploit wind power as well as problems that may rise.
- **Chapter 3** describes the layout of the wind-farm used for identification, it describes how the turbine Vestas $V90-3$MW is composed and the available measurements.
- Inside **Chapter 4** the concept of *Effective Wind Speed* is introduced, a quick overview on the Extended Kalman Filter is given: algorithm used to compute Effective Wind Speed, finally the system turbine is modeled.
- **Chapter 5** describes the interactions that occur in a wind farm, it explains what the wake effect is, its consequences and introduces an hypothesis on the model to be used in the identification section.

- **Chapter 6** describes 2 different methodologies adopted to identify the model we were looking for and it shows which one is giving better results and why.
- In **Chapter 7** the model formerly computed are validated adopting an iterative process. A predictor is calculated starting from the model structure chosen in the validation step.
- The predictor computed is used in **Chapter 8** in a possible (very simple) control scheme, showing improvements and drawbacks of this solution.
- In **Chapter 9** conclusions are shown and possible future developments are suggested.

Chapter 2

Wind Origin And How To Exploit It

2.1 Wind Origin

Wind consists of the movement of gases on a very large scale. On the Earth, wind is represented by the free flow of air. Winds are classified by their speed, their spatial scale, their effects, the forces that cause them and the regions in which they occur. In meteorology, winds are referred to according to the direction from which the wind is blowing and according to their strength. With the name gusts are intended short bursts of high speed wind. Strong winds of intermediate temporal length are termed squalls. Long-duration winds are called in different ways that vary according to their average strength: breeze, gale, storm, hurricane, and typhoon. Wind happens on a range of different scales: thunderstorms lasting tens of minutes, local breezes due to the heating of land surfaces with average duration of a few hours, global winds caused by the different absorption of solar energy between the climatic zones on Earth[2].
Wind is caused by differences in pressure: if a difference in pressure exists, the air moves, accelerating, from higher to lower pressure. Because of the rotation of the planet, the air will be deflected by the Coriolis effect, except on the equator. The two biggest driving factors of large-scale winds (the atmospheric circulation) are the rotation of the planet and the different heating rates between the equator and the poles. Outside the tropics and far away from the surface, where frictional effects can be disregarded, the large-scale winds tend to approach geostrophic balance, that is when the force of pressure is balanced by the Coriolis force:[2]

$$\begin{cases} -f_v = -\dfrac{1}{\rho}\dfrac{\partial p}{\partial x} \\ f_u = -\dfrac{1}{\rho}\dfrac{\partial p}{\partial y} \end{cases} \tag{2.1}$$

Near the Earth's surface, friction causes the wind to be slower than it would be otherwise. Surface friction also causes winds to blow more inward into low pressure areas[3].
From the point of view of wind energy, the most important characteristic of the wind is its variability. The wind is highly variable, both temporally and geographically. Furthermore this variability holds over a very wide range of scales in space and time. Spatial variability justifies the existence of different climatic regions in the world, some characterized by higher winds than others. These regions are largely influenced by the latitude, which affects the amount of solar energy that can be captured. Also within the same climatic region there are differences due to physical geography (proportion of land and sea, presence of mountains, type of vegetation etc.). At a given location, temporal variability on a large scale refers to the fact that the amount of wind may vary from year to year, with even larger variations over periods of decades or more. These long-term variations are not fully understood. On periods shorter than a year, seasonal variations are more predictable. On still shorter time-scales, ranging from minutes down to seconds or less there exist wind-speed variations known as turbulence. These can have a very significant effect on the design and performance of the individual wind turbines, as well as on the quality of power delivered to the network and its effect on consumers[7].

2.2 Wind Energy

It is possible to exploit the kinetic energy of the air in motion to produce electrical energy. If we consider an imaginary area A, the total wind energy flowing through this area during time t is:

$$E = \frac{1}{2} A v t \rho v^2 \tag{2.2}$$

being ρ the air density, v the velocity and Avt the volume of air passing through A, perpendicular to the velocity. The total wind power for a given velocity is $P = E/t$, that is:

$$P = \frac{1}{2} \rho A v^3 \tag{2.3}$$

proportional to the third power of the velocity.
Total wind power could be captured only if the wind velocity is reduced to zero. In a realistic wind turbine this is impossible, as the captured air must also leave the turbine. A relation between the input and output wind velocity must be considered. Using the concept of stream tube, the maximal achievable extraction of wind power by a wind turbine is 59% of the total theoretical wind power (Betz limit)[7]. Further insufficiencies, such as rotor blade friction and drag, gearbox

losses, generator and converter losses, reduce the power delivered by a wind turbine. Anyway the basic relation that the turbine power is (approximately) proportional to the third power of velocity remains. The ratio between turbine power and wind power is known as aerodynamic efficiency and represents the turbine's power coefficient C_p. This coefficient varies with the tip speed ratio, λ, (the ratio of rotor tip speed to free wind speed) and with the pitch angle, β, so

$$\begin{aligned} C_p &= C_p(\lambda, \beta) \\ \lambda &= \frac{\omega R_r}{v}. \end{aligned} \tag{2.4}$$

Incremental improvements in the power coefficient are continually being sought by detailed design changes of the rotor and, by operating at variable speed, it is possible to maintain the maximum power coefficient over a range of wind speeds. However, these measurements will give only a modest increase in the power output. Major increases in the output power can only be achieved by increasing the swept area of the rotor or by locating the wind turbines on sites with higher wind speeds.

Chapter 3

Thanet Description

3.1 Site Description

The aim of this work is to look for the possibility of predicting wind speed at one turbine, knowing the wind speed at the previous turbine. In order to do this, several measurements recorded through a SCADA system from Thanet wind farm have been used. Thanet wind farm is an offshore wind farm located 11km off the cost of Thanet district in Kent, England (Figure 3.3).

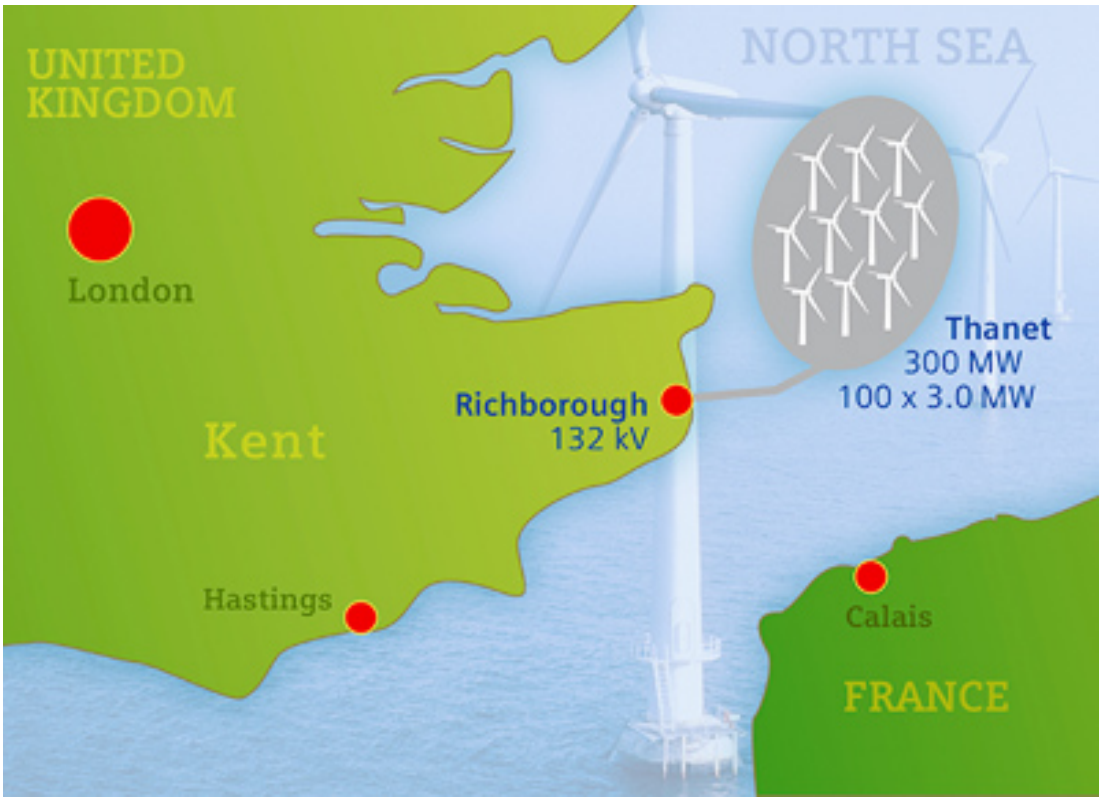

Figure 3.1: Location of Thanet Wind Farm

It is the world's second largest offshore wind farm. The Thanet project is composed of 100 Vestas $V90-3$MW turbines, with 480m between turbines and 715m between the rows. It generates 960GWh per year and, by yearly average, is sufficient to supply approximately 240,000 homes. Two submarine power cables run from an offshore substation within the wind farm connecting it to an onshore substation in Richborough, Kent. The offshore substation steps up the turbine voltage of 33kV to 132kV for the grid.
The layout of the wind farm is shown in Figure 3.2.

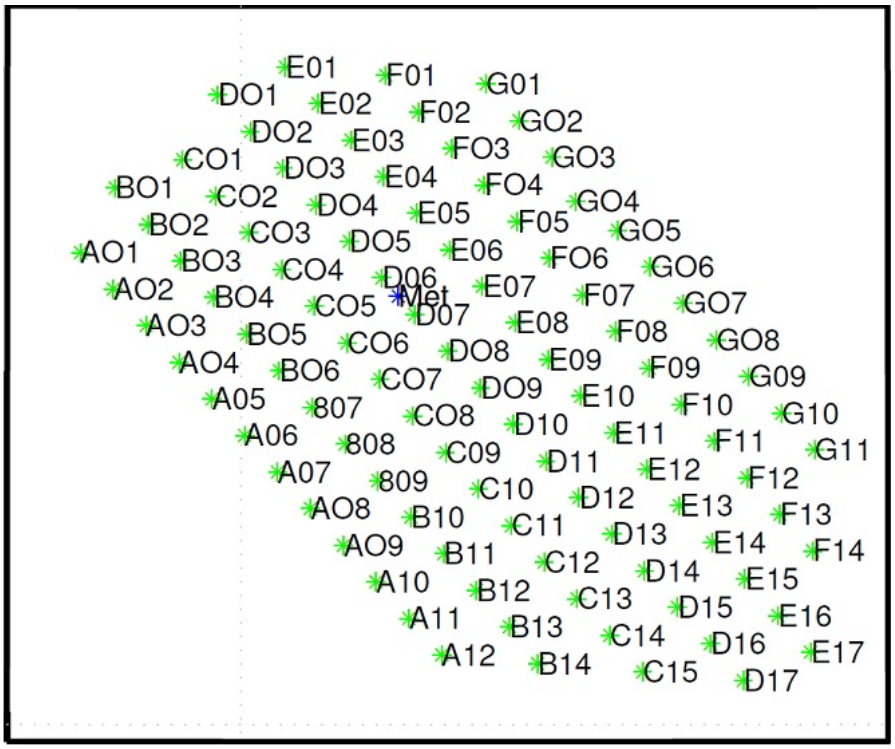

Figure 3.2: Layout of Thanet Wind Farm

Measurements available come from turbines $A01$ to turbine $A08$ and from turbines $B03 - B04$, sampled at 1Hz and are shown in Table 3.1.

3.2 $V90$ Description

The Vestas $V90 - 3$MW is a new generation, variable speed, three-bladed upwind turbine (Figure 3.3).

Figure 3.3: Vestas $V90$ turbine

This turbine is composed of a 90m high tower, on top of which is located the nacelle that is the casing for a doubly fed induction generator, low speed and high speed shafts, gearbox, controller and other required instrumentation. The nacelle can rotate to be oriented towards the wind (yaw control). In the front there is mounted the three-bladed rotor whose blades are 45m long and can rotate on their axis in order to control tower vibration and/or produced power (pitch-control).

Wind turbine	Measure
	Generator RPM
	Nacelle Direction
	Pitch Angle
	Power
	Power Reference
	Rotor RPM
	System State
	Tower Acc Long
	Tower Acc Trans
	Wind Direction
	Wind Speed
Met. Mast	**Measure**
	Air Temperature
	Wind Direction
	Wind Speed

Table 3.1: Measurement specifications

Chapter 4

Effective Wind Speed

4.1 Introduction

Wind speed is, in general, a vector field $V : \mathbb{R}^4 \to \mathbb{R}^3$[15], in fact wind speed varies both with time and space. Measurements provided by the wind ultrasonic sensors are not affordable since the area swept by the rotor is $A_r = \pi R_r^2 \approx 6362\text{m}^2$ while the anemometer provide something that compared to A_r looks like a punctual measurement. Of course the wind measurements provided is correlated to the wind hitting the turbine, but there can be discrepancies in wind speed among points located sufficiently far away from the anemometer.
Light detection and ranging technique would be an option to measure a profile of the real wind some meters in front of the turbine, but this is not part of standard signals available on the turbine and it is also expensive. In order to overcome this the **Effective Wind Speed** concept (EWS) is introduced:

with Effective Wind Speed we refer to an imaginary wind that, when hits the turbine, would produce the same power produced by the real wind that hits the turbine.

The advantage of using this imaginary wind is that it is constant over the rotor area, even though it still varies with time and is less noisy than the measured one (EWS represents the wind field averaged over the rotor area), also referred to as **Nacelle Wind Speed** (NWS).

4.2 Effective Wind Speed Estimation

In order to estimate this quantity, a continuous-discrete Extended Kalman Filter is used[15], since an estimation of the input of the system is needed and also because it takes advantage of nonlinear time varying turbulence model. A continuous-discrete Extended Kalman Filter has been chosen since the system

lends itself to continuous modeling while available measurements are at discrete time. The algorithm is governed by the following equations:

$$\begin{cases} \dot{\hat{\mathbf{x}}}(t) = f(\hat{\mathbf{x}}(t), \mathbf{u}(t)) \\ \dot{\mathbf{P}}(t) = \mathbf{F}(t)\mathbf{P}(t) + \mathbf{P}(t)\mathbf{F}(t)^T + \mathbf{Q}(t) \end{cases} \tag{4.1}$$

with:

$$\begin{cases} \hat{\mathbf{x}}(t_{k-1}) = \hat{\mathbf{x}}_{k-1|k-1} \\ \hat{\mathbf{P}}(t_{k-1}) = \hat{\mathbf{P}}_{k-1|k-1} \end{cases} \tag{4.2}$$

$\mathbf{F}$ matrix is obtained through linearization of the system equations.
Update of the filter is obtained in the following way:

$$\begin{cases} \mathbf{K}_k = \mathbf{P}_{k|k-1}\mathbf{H}_k^T(\mathbf{H}_k\mathbf{P}_{k|k-1}\mathbf{H}_k^T + \mathbf{R}_k)^{-1} \\ \hat{\mathbf{x}}_{k|k} = \hat{\mathbf{x}}_{k|k-1} + \mathbf{K}_k(\mathbf{y}_k - h(\hat{\mathbf{x}}_{k|k-1} \\ \mathbf{P}_{k|k} = (\mathbf{I} - \mathbf{K}_k\mathbf{H}_k)\mathbf{P}_{k|k-1} \end{cases} \tag{4.3}$$

where matrix $\mathbf{H}$ is obtained by linearizing the output transformation[6]. The EKF algorithm uses a Runge-Kutta 4 algorithm ($RK4$) to predict the next state vector and covariance matrix and then uses the linearized matrices to refine the estimates. It takes the following inputs:

- state equations (f);
- output equations (h);
- state linearization ($dfdx$);
- output linearization ($dhdx$);
- state dimension (n);
- input vector (U);
- output vector (Y);
- initial state and covariance matrix ($x0 - P0$);

- process and output variance matrices ($Q - R$);

- sample time (Ts);

- number of steps to use in ($RK4$) (Ii).

and returns as outputs:

- State prediction x(n|n-1) (XHM);

- State estimate x(n|n) (XHP);

- Output prediction y(n|n-1) (YHM);

- Kalman gain matrices with time as third index ($KRes$);

- Covariance estimate matrices with time as third index ($PpRes$).

Pseudocode fore the EKF algorithms follow:
Algorithm 4.2.1: EKFCD$(f, h, dfdx, dhdx, n, U, Y, x0, P0, Q, R, Ts, Ii)$

$xhm \leftarrow x0;$
$u0 \leftarrow U(:,1);$
$yhm \leftarrow h(xhm, u0);$
$Pm \leftarrow P0;$
$A \leftarrow dfdx(xhm, U(:,1));$
$C \leftarrow dhdx(xhm, U(:,1));$
$N \leftarrow length(U);$

for $i \leftarrow 1$ **to** N
do
$XHM(:,i) \leftarrow xhm;$
$YHM(:,i) \leftarrow yhm;$
$PmRes(:,:,i) \leftarrow Pm;$
$PymRes(:,:,i) \leftarrow C * Pm * C' + Rv;$
$C \leftarrow dhdx(xhm, U(:,i));$
$K \leftarrow Pm * C'/(C * Pm * C' + Rv);$
$xhp \leftarrow xhm + K * (Y(:,i) - yhm);$
$XHP(:,i) \leftarrow xhp;$
$Pp \leftarrow (eye(n) - K * C) * Pm * (eye(n) - K * C)' + K * Rv * K';$

if $any(eig(Pp) < 0)$
then
$error$

else $KRes(:,:,i) \leftarrow K;$
$PpRes(:,:,i) \leftarrow Pp;$
$xhm \leftarrow xhp;$
$Pm \leftarrow Pp;$
$Pm \leftarrow Pm + RungeKutta4Method(Pm);$
$xhm \leftarrow xhm + RungeKutta4Methog(xhm);$

if $any(eig(Pm) < 0)$
then
$error$

else
$yhm \leftarrow h(xhm, U(:,i+1));$

return $(XHM, XHP, YHM, KRes, PpRes)$

4.3 Turbine Model

In order for the EKF algorithm to work a model of the system must be provided. In Figure 4.1 it is possible to see an insight of a wind turbine.

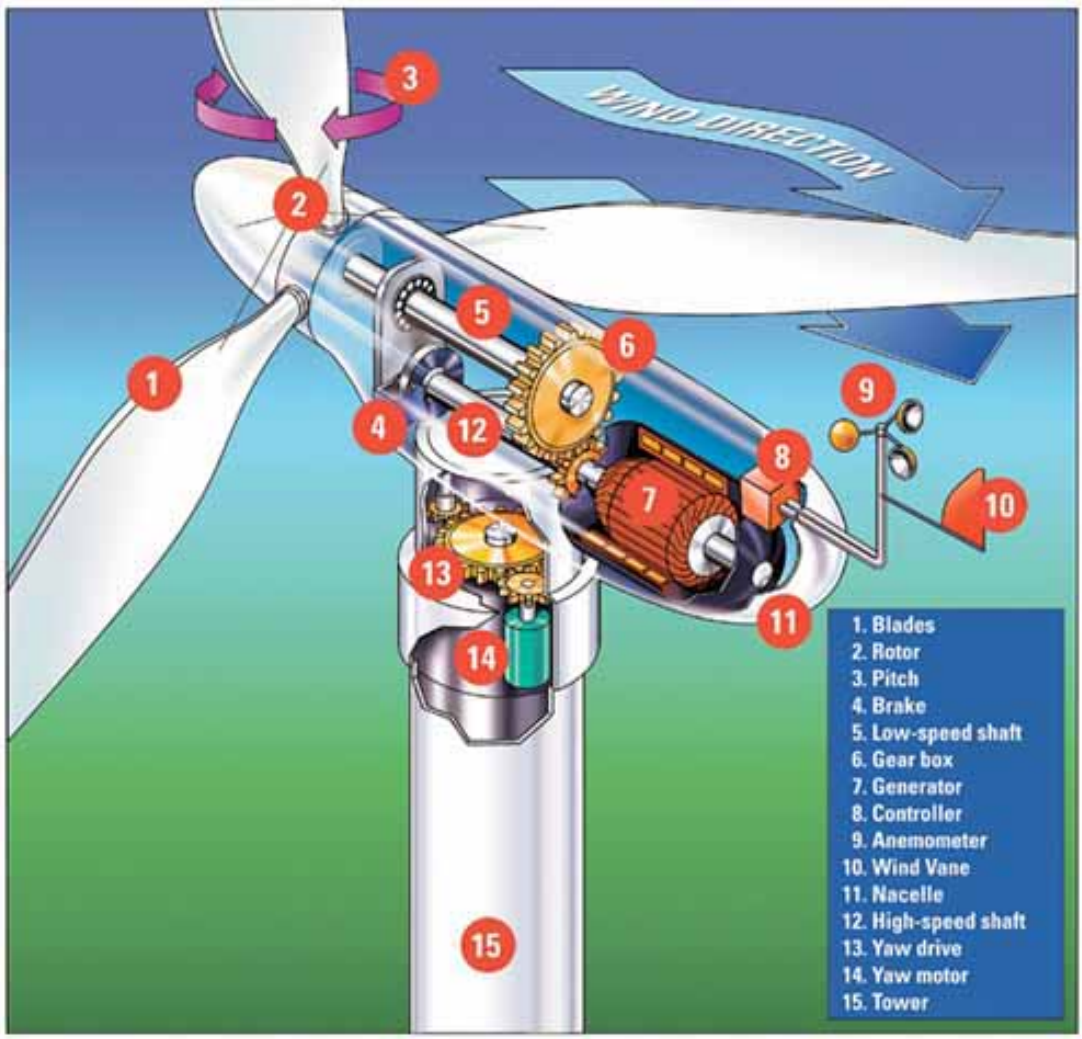

Figure 4.1: Wind turbine insight

The turbine consists of a rotor whose inertia is J_r, connected to a low speed shaft, supposed to be stiff, which is linked through an elastic transmission (with elastic constant K_s, damping B_s, gear ratio N) to a high speed shaft. This shaft is connected to a doubly fed induction generator (with inertia J_g). These machineries are contained in a nacelle mounted on the top of an elastic tower (mass M_n, elastic constant K_t, damping B_t). If we think about how this process works, it can be seen that the wind is accelerating the rotor through the aerodynamic torque. Thanks to the transmission also the high speed shaft rotates at a cer-

tain velocity which, at steady state, is $N\omega_r$ and is the same velocity available on the generator. A torque opposed in direction to the rotational speed is used to control the the rotor velocity. The wind is also causing the tower to vibrate. This vibration actually affects the available wind speed at the rotor depending on the direction of the vibration. The system turbine shown in Figure 4.1, with reference to the nacelle, can be seen as a 2 degree of freedom rotational mechanical system. In order to better understand it, it is possible to refer to Figure 4.2 where a system of the same kind is shown in a more simple way.

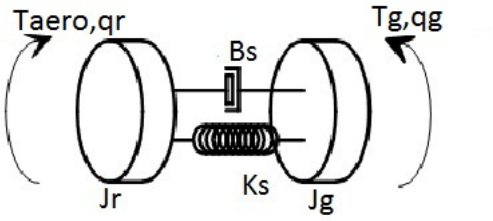

Figure 4.2: Simple schematic of the system

The equations governing it are:

$$\begin{aligned} J_g\ddot{q}_g + K_f\dot{q}_g &= -T_g + \frac{1}{N}T_{r-g} \\ J_r\ddot{q}_r &= T_r - T_{r-g} \\ T_{r-g} &= K_s(q_r - \frac{1}{N}q_g) + B_s(\dot{q}_r - \frac{1}{N}\dot{q}_g) \end{aligned} \tag{4.4}$$

Where q_g, q_r are the angular positions respectively of the generator and of the rotor. J_g, J_r are the inertias, N is the gearbox ratio, K_f is the friction, considered to be acting only on generation side and depending on velocity; finally K_s, B_s are the stiffness and damping of the transmission flexibility. By introducing the displacement angle $\phi = q_r - \frac{1}{N}q_g$, calling rotor and generator velocity respectively $\omega_r = \dot{q}_r$, $\omega_g = \dot{q}_g$ and assuming a second order lumped parameters description for

the tower, the system can be modeled as follow:

$$\begin{cases} \dot{\omega}_r = \frac{1}{J_r}(\frac{1}{2}\rho A_r(V_e - d_{n2})^3 C_P(\lambda,\beta)\frac{1}{\omega_r} - K_s\phi - B_s\dot{\phi}) \\ \dot{\omega}_g = \frac{1}{J_g}(-\frac{P_g}{\mu\omega_g} - K_f\omega_g + \frac{1}{N}(K_s\phi + B_s\dot{\phi})) \\ \dot{\phi} = \omega_r - \frac{1}{N}\omega_g \\ \dot{d}_{n1} = d_{n2} \\ \dot{d}_{n2} = -\frac{B_t}{M_n}d_{n2} - \frac{K_t}{M_n}d_{n1} + \frac{1}{2M_n}\rho A_r C_T(\lambda,\beta)(V_e - d_{n2})^2 \end{cases} \tag{4.5}$$

Basically, with this description of the tower, the nacelle is considered to be moving horizontally, with no changes in the height. This horizontal movement actually affects the intensity if the wind hitting the rotor, since if wind speed and vibration velocity d_{n2} have the same direction the aerodynamic torque available is reduced while if they have opposite direction the torque is increased. This explains why in the expression of the aerodynamic torque the term $V_e - d_{n2}$ appears. If we analyze the system modeled so far with the physical constants of $V90-3\text{MW}$ in the equations, a couple of complex conjugate zeros-poles (due to the transmission) appear at a frequency $\omega_{tr} \approx 10.5\text{rad/s}$. Since the sampling frequency is $f_s = 1\text{Hz}$ this contribution can be disregarded and the system can be modeled as a fully rigid one. Disregarding the transmission in (4.5) leads to the following model:

$$\begin{cases} \dot{\omega}_r = \frac{1}{J_r + J_g N^2}(\frac{1}{2}\rho A_r(V_e - d_{n2})^3 C_p(\lambda,\beta)\frac{1}{\omega_r} - NT_g - NT_f) \\ \dot{d}_{n1} = d_{n2} \\ \dot{d}_{n2} = -\frac{B_t}{M_n}d_{n2} - \frac{K_t}{M_n}d_{n1} + \frac{1}{2M_n}\rho A_r C_t(\lambda,\beta)(V_e - d_{n2})^2 \end{cases} \tag{4.6}$$

V_e represents the wind speed, that is the input we need to estimate. In order to do so, we enlarge the mechanical system adding as many states as necessary to describe this input.
The process wind can be decomposed into two states: the first one describing the mean wind speed and the second one describing the turbulence around the mean wind speed. The model chosen is the following:

$$\begin{cases} \dot{v}_t = -\frac{v_m\pi}{2L}v_t + n_1 \\ \dot{v}_m = n_2 \end{cases} \tag{4.7}$$

Also a model for the noise is needed: the mean wind speed should be able to vary slowly from zero to at least 25m/ sec, value that represents the turbine cut out wind speed. If we assume that the standard deviation of mean wind speed over

10 min is 2m/ sec we can set n_2 to $\frac{2^2}{600}$. As regards the process noise affecting the turbulent part we can describe it as:

$$n_1 = \frac{v_m^3 t_i^2 \pi}{L}. \tag{4.8}$$

This comes from requiring the same peak frequency and variance as obtained by the Kaimal spectrum. The turbulent part is known to vary with mean wind speed, this explains the dependency of the dynamic and variance via v_m[7, 15]. Parameter t_i is known as turbulence intensity and is a measurement of the overall level of turbulence. It is defined as:

$$t_i = \frac{\sigma}{\bar{U}} \tag{4.9}$$

where σ is the standard deviation of wind speed variations about the mean wind speed $\bar{U}$, usually defined over 10 minutes. The turbulence intensity depends on the roughness of the surface and the height above the surface. It also depends on the presence of hills or mountains (especially if they lie upwind) and on the thermal behavior of the atmosphere. Anyway as the height above ground increases, the effects of all these processes become weaker. Above a certain height, the air flow can be considered largely free of surface influences[7].
Said this, it is possible to define the driving input of the turbine V_e as:

$$V_e = v_m + v_t. \tag{4.10}$$

L is known as length scale parameter, it also depends on the surface roughness, but far enough above the ground it becomes more or less constant and isotropic, with a value $L = 140$m. The complete system, augmented with the wind equations looks like:

$$\begin{cases} \dot{\omega}_r = \dfrac{1}{J_r + J_g N^2}(\dfrac{1}{2}\rho A_r (V_e - d_{n2})^3 C_p(\lambda, \beta)\dfrac{1}{\omega_r} - NT_g - NT_f) \\ \dot{d}_{n1} = d_{n2} \\ \dot{d}_{n2} = -\dfrac{B_t}{M_n} d_{n2} - \dfrac{K_t}{M_n} d_{n1} + \dfrac{1}{2M_n}\rho A_r C_T(\lambda, \beta)(V_e - d_{n2})^2 \\ \dot{v}_t = -\dfrac{v_m \pi}{2L} v_t + n_1 \\ \dot{v}_m = n_2 \\ V_e = v_m + v_t \\ \lambda = \dfrac{\omega_r R_r}{V_e} \end{cases} \tag{4.11}$$

As regards the output transformation, if we look at the measurements available and we think about how the turbine works it's easy to see that:

- the produced power constitutes an input for the system, since from it the control torque of the generator can be derived as:

$$T_g = \frac{P_g}{\eta_{gen}\eta_{transm}\omega_g}; \tag{4.12}$$

- the pitch angle β is an input of the system, since by varying it, both C_p and C_t coefficients vary and is then possible to control the output;

- both rotor and generator velocity can be controlled either by acting on T_g or β. Since the system is modeled as a fully rigid one reduced to the rotor ω_r constitutes and output for the system;

- the nacelle wind speed, whose measurements are available, can be seen as a very noisy and uncertain measurement of V_e.

Provided this, the output transformation looks like:

$$\begin{cases} y_1 = \omega_r + v_1 \\ y_2 = v_m + v_t + v_2 \end{cases} \tag{4.13}$$

Since this model will be used in an EKF algorithm, it is required that the couple (A, C), with $A = \frac{\partial f}{\partial x}$ and $C = \frac{\partial h}{\partial x}$ is observable or, at least, detectable[19]. This condition always stands, however the condition number for the observability matrix of the 5 states system is high (≥ 300), probably because of the lack of direct measurements of tower oscillation[15]. Tower measurements provided by Vestas could not be used because of mismatches between model and real system: according to the tower model adopted, mass, damping and elasticity supplied, the natural frequency of the tower should lie at 0.24Hz while a spectral analysis of the tower acceleration, both in X and Y direction shows a peak at 0.36Hz which corresponds to an error of 50% more than what was expected. This mismatch in the natural frequency of the tower $\omega_n = \frac{K_t}{M_n}$ is probably due to an incorrect value of the tower stiffness K_t. An estimation problem could have been set also for this parameter but since the stiffness can be influenced by meteorological conditions that change over time it was preferred to disregard the tower contribution, that is small, rahter than dealing with a system that could have been time-variant. Because of this reason a 3 states model, with the tower dynamic neglected has been used. Being 4.13 the output transformation the complete system used for

identification looks like:

$$\begin{cases} \dot{\omega}_r = \dfrac{1}{J_r + J_g N^2}\left(\dfrac{1}{2}\rho A_r V_e^3 C_p(\lambda,\beta)\dfrac{1}{\omega_r} - NT_g - NT_f\right) \\ \dot{v}_t = -\dfrac{v_m \pi}{2L} v_t + n_1 \\ \dot{v}_m = n_2 \\ y_1 = \omega_r + v_1 \\ y_2 = v_m + v_t + v_2 \\ V_e = v_m + v_t \\ \lambda = \dfrac{\omega_r R_r}{V_e} \end{cases} \tag{4.14}$$

Since it was assumed that measurement noise on rotor speed is approximately 2% and on Nacelle Wind Speed is large because of blades passing by[15], measurement noise has been set to:

$$R = \begin{pmatrix} 0.02 & 3 \end{pmatrix} \tag{4.15}$$

Also algorithm's initial state x_0 and initial (diagonal) covariance matrix P_0 is as follow (being σ_i the standard deviation of the whole measurement set i):

$$x_0 = \begin{pmatrix} \omega_r(0) & 0 & Nws(0) \end{pmatrix} \tag{4.16}$$

$$P_0 = diag\begin{pmatrix} \sigma^2_{\omega_r} & 0.2 & \sigma^2_{Nws} \end{pmatrix} \tag{4.17}$$

Estimation results for turbine $A01$ are shown in Figure 4.3 and are compared with the nacelle measurements. In order to validate the estimated EWS sequences, its

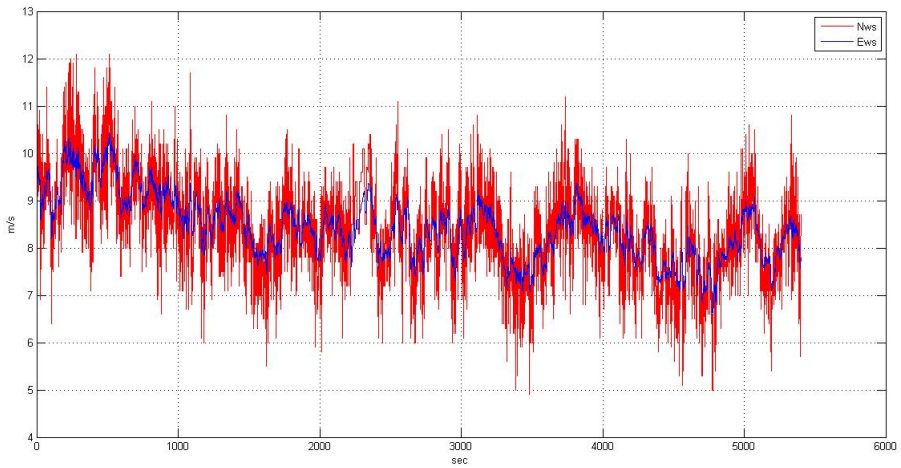

Figure 4.3: Nacelle wind speed (red) vs Effective wind speed (blue)

definition has been applied. If the estimated wind really represents the one hitting

the rotor than the power output should be the same. Through a simulation it has been possible to see that EWS sequences produce a power output similar to the measured one.Figure 4.4 The power output produced by NWS instead has a magnitude and shape that differs from the measured one, confirming the starting hypothesis of unreliability Figure 4.5.

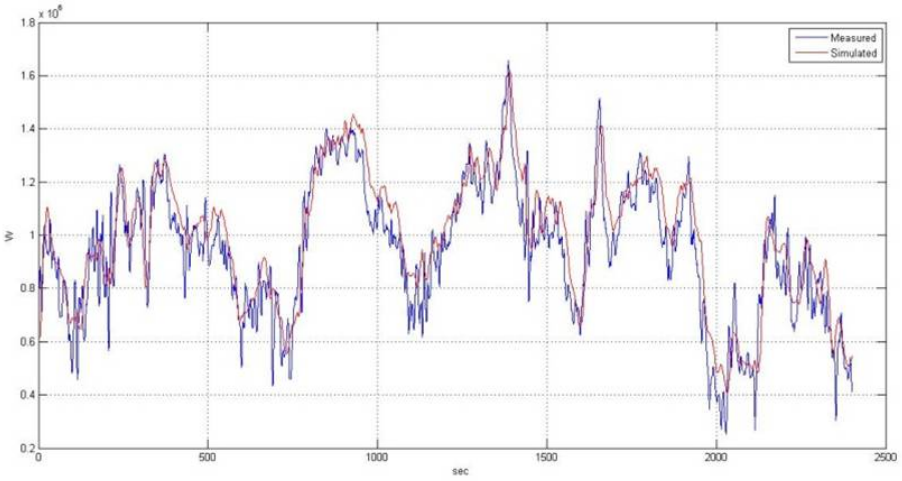

Figure 4.4: Real produced power (blue) vs. simulated one (red)

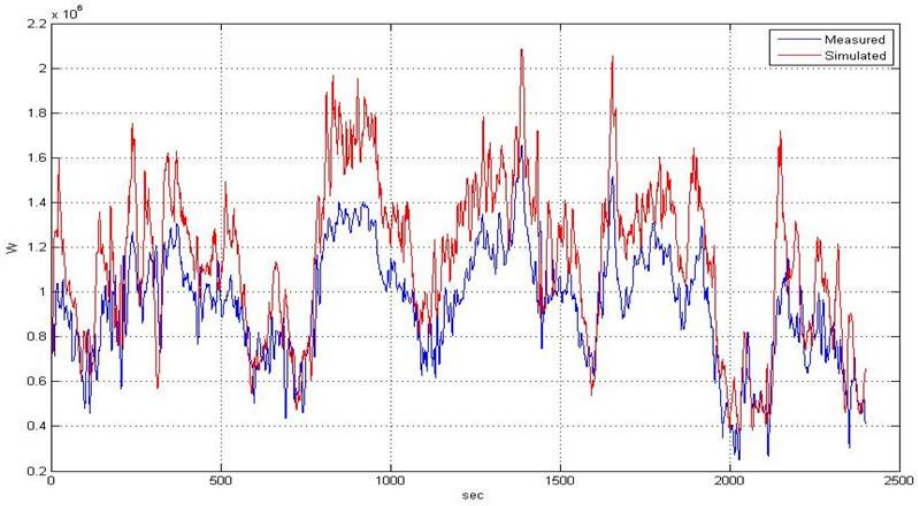

Figure 4.5: Real produced power (blue) vs. simulated one (red)

Chapter 5

Wind Model Hypothesis

In the estimation of EWS described in chapter 4, sequences of wind speed blowing in direction NNW, approximately around 320° have been used. This means that the wind is traveling along the columns of the wind farm from turbine 01 to turbine 08. Along its way, it encounters several transformations due to interactions with the turbines as it is illustrated in the simplified Figure 5.1 As

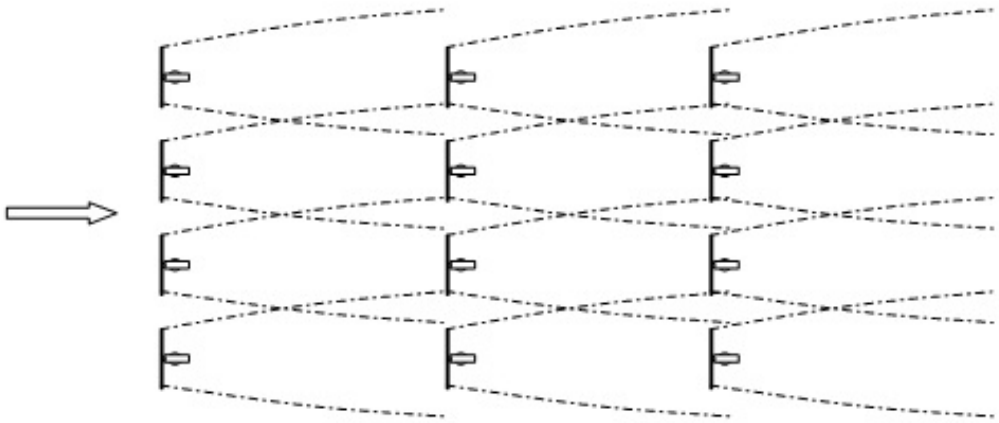

Figure 5.1: Interaction between turbines in a wind farm

a result of the interaction shown, wind speed decreases while turbulence (wake effects) increases. The correct study of the wake effect gives the possibility to control and adjust the shadowing of inner wind turbines, to decrease the wake and to increase the energy yield from the wind farm. The air flux that comes from one turbine to the next one is reduced and becomes turbulent. The wind turbine positioned just behind the first one experiences a reduced and whirled air flow and produces less energy. This phenomenon of shadowing is called wake-

effect[5]. The wake's structure consists of several zones: near wake, intermediate wake and far wake as shown in Figure 5.2. The length of each zone depends on the rotor diameter and its properties are determined by the values of pressure p and wind speed V[13]. The wake propagation phenomenon in a wind farm is such

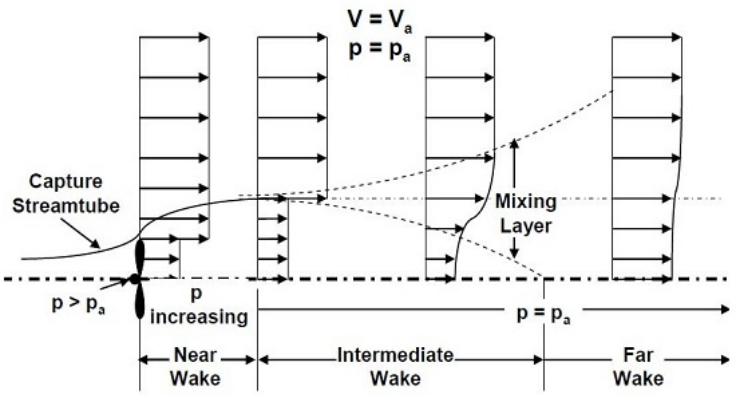

Figure 5.2: Wake flow structure

that the wind speed tend to decrease moving along the turbines while turbulence increases. These modifications anyway tend to approach a steady state characterized by more or less the same (mean) wind speed and turbulence intensity. The major transformations happen between the first two turbines encountered by the wind along its travel, therefore a transition region between the first and second turbine can be defined. Since the wind in this transition zones is subject to deep modifications the model (if existent) that describe this zone should be characterized by high uncertainty in the parameters. From a spectral point of view instead low frequency components travel along the wind farm and may be affected by the presence of obstacles, this means that their magnitude or phase may be changed. High frequency components instead represent turbulent energy which is dissipated into heat and replaced by new eddies completely uncorrelated with the original ones. These considerations suggests a model structure linking $V_{e_{i+1}}$ to V_{e_i} such as the one presented in Figure 5.3, where there can be seen a direct contribution to wind speed $V_{e_{i+1}}$ coming from the previous turbine, plus a noisy contribution that represents the uncorrelated new high frequency components, so that the wind speed spectrum is preserved. Since we refer to linear models, what we really take into account are the variations around a mean value

of wind speeds at turbines. With reference to Figure ?? we can state that:

$$u(t) = V_{e_i} - \overline{V}_{e_i} \quad y(t) = V_{e_{i+1}} - \overline{V_{e_{i+1}}} \tag{5.1}$$

Finally a delay is needed since the wind particles take a finite time to travel along the distance $d = 480$m.

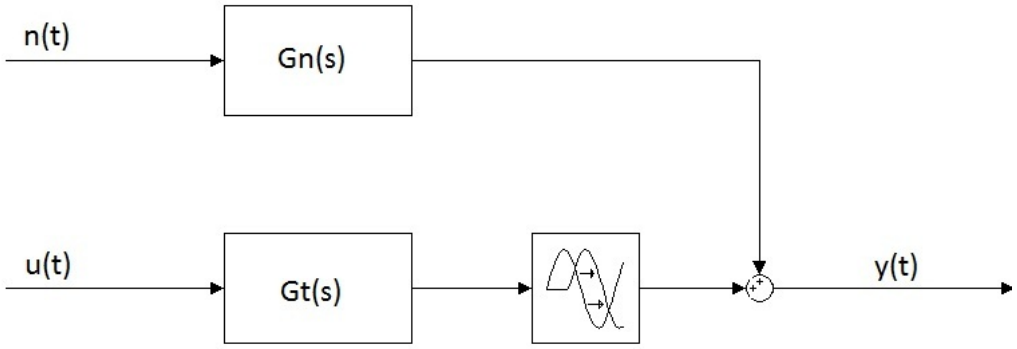

Figure 5.3: Model structure

Chapter 6

Model Identification

6.1 Prediction Error Method Identification

Let's consider a family of models

$$\mathcal{M} = \{M(\theta)|\theta \in \Theta\} \tag{6.1}$$

being θ the vector of the coefficients of the model M. Let's also consider available data as measurements of the input $u(\cdot)$ and of the output $y(\cdot)$ at time instants $t = 1, ..., N$. The problem to solve is to find the model, in the chosen family, that best explains data[19]. The approach chosen is the predictive one, that is as follow: given a family of model, we calculate the associate 1 step predictor which will produce the output

$$\hat{y}(t+1|t) = f(u^t, y^t, \theta) \tag{6.2}$$

being u^t, y^t the sequences $\{u(t), u(t-1), ...\}$ and $\{y(t), y(t-1), ...\}$. In this way it is possible to construct the error sequence:

$$\epsilon_\theta(t) = y(t+1) - \hat{y}(t+1|t) \tag{6.3}$$

and to evaluate the mean error:

$$J(\theta) = \frac{1}{N}\sum_{t=\kappa}^{N} \epsilon(t)^2 \tag{6.4}$$

being κ the first instant when it is possible to evaluate the output prediction from available data. In this way we can build the cost function $J(\theta)$, which depends on the particular set of parameter chosen. Varying the parameters will vary the value of the cost function.

6.1.1 Practical Realization

In order to have this algorithm to work it is necessary to choose a family model and to identify the delay affecting the system. An easy way to estimate

the delay is just to set it as:

$$\tau = \frac{d}{\bar{v}} \tag{6.5}$$

being $d = 480$m and $\bar{v}$ the mean wind speed. This first approach can give only a rough idea of the magnitude of the delay, since wind speed is not constant over time also the delay will vary from sample to sample. Since the models used for identification are time invariant it is better to use a value for the delay that best fits available data. This choice can be done in a almost automatic way by the identification algorithm: the idea is to identify several models, one for each significant delay value inside a certain range Δ, and then to choose the model that shows the lowest FPE value among all. If we construct a statistic for the time-varying delay by binning each sample a more or less Gaussian distribution is obtained as shown in Figure 6.1 The red line in 6.1 represents a Gaussian

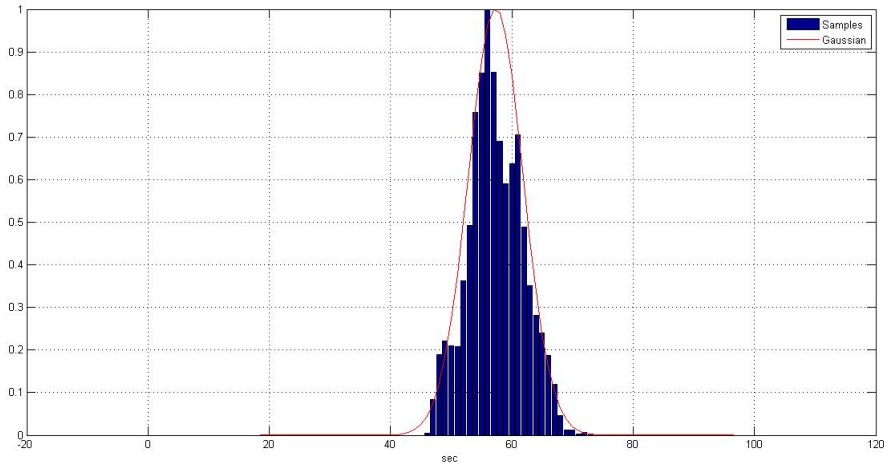

Figure 6.1: Gaussian distribution of the delay

distribution fitted to delay data, in this particular case it is characterized by: $\mathcal{N}(\mu, \sigma^2) = \mathcal{N}(57.3, 20.5)$. The range Δ has been chosen as $\mu \pm \sigma$. The family of models chosen is *Box-Jenkins*, to enforce equal spectral characteristics of the wind at the two turbines. Referring to Figure 5.3, we can in fact assume that:

$$|G_t(j\omega)|^2 |G_u(j\omega)|^2 + |G_n(j\omega)|^2 \approx |G_u(j\omega)|^2 \tag{6.6}$$

where $G_u(j\omega)$ represents the input spectrum while for the noise $n(t)$ it is assumed unitary variance. In case of a more specific model (*ARX*, *ARMAX*, *OE*) it should always be possible, through simplifications, to go back to the correct family. Box-Jenkins model structure is shown in 6.7:

$$y(t) = \sum_{i=1}^{n_u} \frac{B_i(z)}{F_i(z)} u_i(t - \tau_i) + \frac{C(z)}{D(z)} e(t) \tag{6.7}$$

where n_u is the number of input channels. The orders of Box-Jenkins model are defined as follows:

$$\begin{aligned} n_b &: B(z) = b_1 + b_2 z^{-1} + ... + b_{n_b} z^{-n_b+1} \\ n_c &: C(z) = 1 + c_1 z^{-1} + ... + c_{n_c} z^{-n_c} \\ n_c &: D(z) = 1 + d_1 z^{-1} + ... + d_{n_d} z^{-n_d} \\ n_f &: F(z) = 1 + f_1 z^{-1} + ... + f_{n_f} z^{-n_f} \end{aligned} \tag{6.8}$$

[4]. Referring to Figure 3.2 we introduce two indexes: row-index $i = 1, ..., 7$ and column-index $j = A, ..., F$, with the notation $T(i, j)$ we refer to the turbine in position (i, j) in the previous layout. Since wind sequences taken into account blow in direction NNE, which means along the columns from $T(1, \bar{j})$ to $T(8, \bar{j})$ we can assume the following:

- $T(i, \bar{j})$ can affect $T(i + 1, \bar{j})$;
- $T(k, \bar{j})$ cannot affect $T(k + 2), \bar{j}$, with $k = 1, ..., 6$.
- $T(\bar{i}, j)$ cannot affect $T(\bar{i}, j + 1)$
- $T(i, j)$ cannot affect $T(i + 1, j + 1)$

This means that interaction between turbines exists only along the wind direction and between two adjacent turbines while there is no cross interaction between turbines that are not aligned. These hypothesis are also confirmed by the interaction energy6.9 that is very low[17] at lags $\zeta >> \tau$ for turbines that don't respect the previous statements.

$$e_{xy}(\zeta) = \int_{-\infty}^{+\infty} x(t) y^*(t - \zeta) dt \tag{6.9}$$

Asterisk denotes complex-conjugation.
Given the previous hypothesis, the model family and delay interval, the identification procedure can begin. Data preprocessing is required: any trend, if present, must be removed since the model we are looking for should describe how wind speed vary around a mean value. In this particular experiment first 1000 samples are skipped since they represent a transition from a wind speed region characterized by mean wind speed $v_m \approx 10$m/s to another region characterized by $v_m \approx 8.5$m/s. Finally, the remaining data is divided into subsequences of 600 samples each. These subsequences are used for identification (first 600 samples) and validation (next 600 samples).

6.2 Spectra Ratio Method

The delay affecting the system is the most critical parameter to identify: it is extremely variable and therefore it is characterized by a great uncertainty.

A good and reliable estimate of this parameter results in a good and reliable estimate of the other parameters of the model. This is the reason why another, more deterministic, way to identify it is desirable. If we define a cross-correlation function $r_{xy}(k)$ in the following way:

$$r_{xy}(k) = \frac{c_{xy}(k)}{\sqrt{c_{xx}(0)}\sqrt{c_{yy}(0)}} \tag{6.10}$$

$$\begin{cases} c_{xy}(k) = \dfrac{1}{N}\displaystyle\sum_{t=1}^{N-k}(x_t - \overline{x})(y_{t+k} - \overline{y}) \\ c_{xy}(k) = \dfrac{1}{N}\displaystyle\sum_{t=1}^{N-k}(y_t - \overline{y})(x_{t+k} - \overline{x}) \end{cases} \tag{6.11}$$

the delay can be estimated as the positive lag k at which $r_{xy}(k)$ has its maximum since it should represent maximum interaction. Negative lags are not taken into account since, according to the definition of this function, they represent future outputs correlated to the present inputs. Although promising, this approach is not feasible since, if the transfer function $G_t(s)$ has a too low bandwidth (as it seems the case) it can act itself as a delay. Suppose the system to be the following simple linear system:

$$Y(s) = G_t(s)e^{-s\tau}U(s) \tag{6.12}$$

and suppose $G_t(s)$ to have a very low bandwidth, let's say $\omega_{G_t(s)} << \omega_{u(t)}$. Because of the limited bandwidth $G_t(s)$ operates a phase shift that, when evaluating the cross-correlation function between input and output of the system, can be easily interpreted or mistaken for a delay itself. The overall result is an overestimation of the delay if, according to this approach, it is defined as the maximum of $c_{xy}(k)$. Anyway this approach suggested another way (called spectra ratio method or SRM) to identify the underlying models: assuming the model structure shown in Figure 5.3, with noise $n_1 \sim WN(0, \lambda^2)$ it is possible to derive, through study of cross correlation functions, relationships from input to output and from noise to output that allow us to identify the aforementioned functions $G_t(s)$, $G_n(s)$ and the delay τ. In particular, from input to output it's possible to write the following:

$$\begin{aligned} &\gamma_{uy}(\tau_1) = E[u(t)y(t+\tau_1)] = \\ &E[u(t)G_t(s)e^{-s\tau}u(t+\tau_1) + u(t)G_n(s)n_1(t+\tau_1)] = \\ &G_t e^{-s\tau}\gamma_{uu}(\tau_1) \end{aligned} \tag{6.13}$$

while from noise to output the following relationship stands:

$$\begin{aligned} &\gamma_{n_1 y}(\tau_2) = E[n(t)y(t+\tau_2)] = \\ &E[n_1(t)G_t(s)u(t+\tau_2) + n_1(t)G_n(s)n_1(t+\tau_2)] = \\ &G_n(s)\gamma_{nn}(\tau_2) = G_n\lambda^2\delta(t) \end{aligned} \tag{6.14}$$

If we look at these relationships in the frequency domain we have:

$$\begin{aligned}\Gamma_{uy}(\omega) &= \mathcal{F}(\gamma_{uy}(\tau_1)) \\ \Gamma_{n_1y}(\omega) &= \mathcal{F}(\gamma_{n_1y}(\tau_2))\end{aligned} \tag{6.15}$$

In particular, just by focusing on the absolute value of the previous functions, we obtain:

$$\begin{aligned}|\Gamma_{uy}(\omega)| &= |\mathcal{F}(\gamma_{uy}(\tau_1))| = |G_t(s)|\,\Gamma_{uu}(\omega) \\ |\Gamma_{n_1y}(\omega)| &= |\mathcal{F}(\gamma_{n_1y}(\tau_2))| = |G_n(s)|\,\Gamma_{n_1n_1}(\omega) = |G_n(s)|\,\lambda^2\end{aligned} \tag{6.16}$$

It is in this way possible to build empirical transfer functions through ratios of spectra. Let this estimated functions be called $\hat{G}_t(s)$ and $\hat{G}_n(s)$ and let's consider $\hat{G}_t(s)$: thanks to the way this function has been built, no informations on the delay are available, if we now compute an estimation of the cross-correlation $\hat{\gamma}_{uy}(\tau_1)$:

$$\hat{\gamma}_{uy}(\tau_1) = \hat{G}_t(s)\gamma_{uu}(\tau_1) \tag{6.17}$$

in the hypothesis that $\hat{G}_t(s) = G_t(s)$ the only difference between $\gamma_{uy}(\tau_1)$ and $\hat{\gamma}_{uy}(\tau_1)$ will be only a time shift due to the missing delay. This method grants an identification of the real delay affecting the system and also the transfer functions estimated should be accurate. This method works perfectly theoretically but in practice it suffers of some problems: since data amount is finite it is not possible to compute the **spectra** of cross and auto correlation functions, but **spectrograms** are computed. Spectrograms are known to be noisy approximations of spectra since they are defined only at frequencies $n\Delta\omega$ (being $\Delta\omega = \frac{1}{T}$, T the total observation time and n is the number of samples available). Of course at these frequencies they coincide with the spectra but the final result is distorted and irregular [18]. Because of these limitations this method applied to the same identification sequences used in previous *Prediction Error Methods* would eventually produce noisy estimates that can hardly be interpreted as transfer functions. Also windowing and smoothing techniques of spectrogram do not help in reducing the noise affecting the estimates.

To overcome this problem it is necessary to approximate separately the magnitude of the spectrograms so far produced before performing their ratio. By looking in a x-semilogarithmic plot, it is possible to see that the shape of the magnitudes resembles the shape of transfer functions with a certain gain G_0 and a number υ of real poles as in Figure 6.2 It seems to be possible to evaluate these transfer functions (call them $\widetilde{\Gamma}_{uu}(s)$, $\widetilde{\Gamma}_{uy}(s)$) by looking separately at the low frequency and high frequency parts and by approximating them with straight line it is possible to produce non-noisy estimates of the spectra.

Reducing the number of samples taken into account to calculate the spectrograms from the whole set available (5400 samples) to the same subsets used in

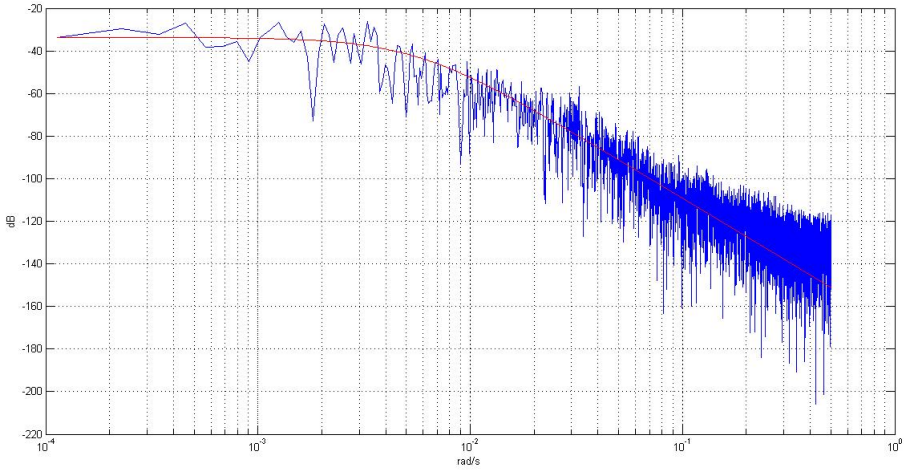

Figure 6.2: Comparison between $\Gamma_{uu}(\omega)$ and its approximation in a semilogarithmic plot

the previous method (600 samples per subsequence) also reduces their reliability at low frequency i.e. it is difficult to define a suitable dc-value. To overcome this problem, considering the shape of wind speed spectra (Figure 6.3), it has been chosen to define this value as the maximum value of the magnitude of the spectrum. The pole position is defined as the particular frequency at which the

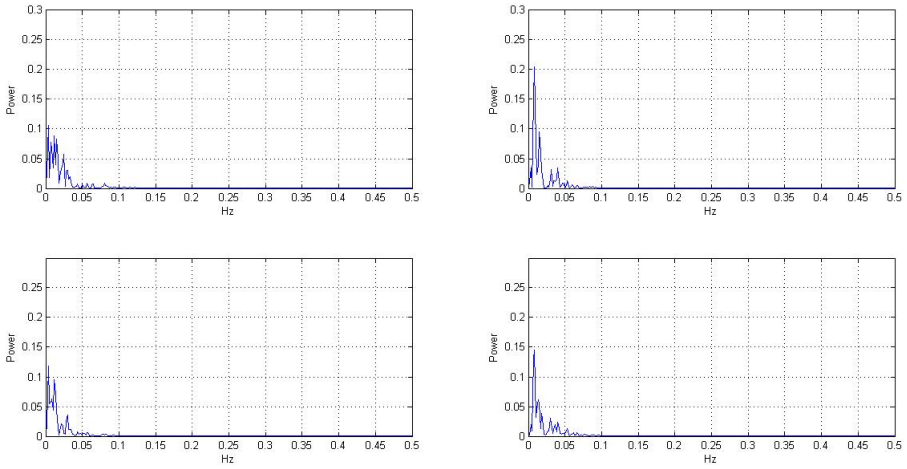

Figure 6.3: Spectra of several wind speed measurements

intersection between low frequency and high frequency straight lines occur, the number of poles has been defined by looking at the steepness of the spectra over a decade. By exploiting the relationships in 6.16 we can define functions $G_t^{(i)}(s)$,

$G_n^{(i)}(s)$ (where i refers to the input/output subsequences taken into account) as:

$$\begin{aligned} \left|\widetilde{G}_t^{(i)}(s)\right| &= \frac{\left|\widetilde{\Gamma}_{uy}^{(i)}(j\omega)\right|}{\widetilde{\Gamma}_{uu}^{(i)}(\omega)} \\ \left|\widetilde{G}_n^{(i)}(s)\right| &= \frac{\left|\widetilde{\Gamma}_{n_1 y}^{(i)}(j\omega)\right|}{\lambda^2} \end{aligned} \tag{6.18}$$

Let's suppose these estimation to be perfect. If we compute $\widetilde{\gamma}_{uy}(\tau) = \widetilde{G}_t(s)\gamma_{uu}(\tau)$ its only difference from $\gamma_{uy}(\tau)$ will be the time delay. This parameter can now be defined as the time-shift between 2 peaks of these cross-correlation functions. Of course the more the previous estimate of the transfer functions $\widetilde{G}_t^{(i)}(s)$ is poor the more the estimate of the delay is not precise.

Chapter 7

Model Validation and Predictor Calculation

7.1 Problem Description

In this part of the work a data set different from the one set used for identification is used to find out if the model taken into account is describing correctly the system dynamics (in the particular case of PEM models, because of how the experiment has been set, also the best order and consequently the best delay are chosen in this session). Validation is required as proof for the model to describe the underlying reality also in cases that it differs from the one on which it was calculated. A data set different from the identification one is needed since being $J(\theta)$ an index of adherence of the model defined by θ to identification data, and being $\hat{\theta}_N$ the minimum of $J(\theta)$ we can assume $J(\hat{\theta}_N)$ to be the index of adherence of the optimal model to data, with N number of free coefficients. This figure of merit is not reliable since it evaluates the goodness of the model on the same data set on which the model has been calculated, and it is clear that $J(\hat{\theta}_N)$ will decrease with increasing complexity since the higher degree of freedom on parameters will step up its adherence to **that** data set. On the other hand its closeness to a particular set of measurements will bind the model to it, jeopardizing its behavior on different sets[18]. The problem to solve now is to find the optimal N and to show that the model shown is consistent that is: the uncertainty on its parameters is low and that it can produce good estimations of the output.

7.2 Problem Solution For PEM Models

Since the previous phase returns several models for each input/output subsequence for each pair of turbines the first problem to solve is to find a model to validate in this set. It has been decided to candidate to the validation phase the

model which has the lowest *Final Prediction Error* (or FPE):

$$FPE(n) = E[\overline{J}(\hat{\theta}_N(s))] = \frac{N+n}{N-n} J(\hat{\theta}_N)^{(n)} \tag{7.1}$$

being n the model order. The best complexity and delay correspond to a value of n for which FPE has a minimum. Since during identification models's orders were allowed to vary between 1 and 2, while the delay was allowed to vary between $\lfloor \mu \pm \sigma \rceil$ and said Δ this interval, the number of models for each sequence is $K = 2 \times 2 \times 2 \times \Delta$. FPE criterion is used to choose the candidate best model complexity among this set, in order to elect the candidate model as the best one available a parameter analysis and a residual analysis are performed. If the candidate model does not pass one of the two steps it is discarded and this procedure is started again from scratch since convergence as in Figure 7.1.

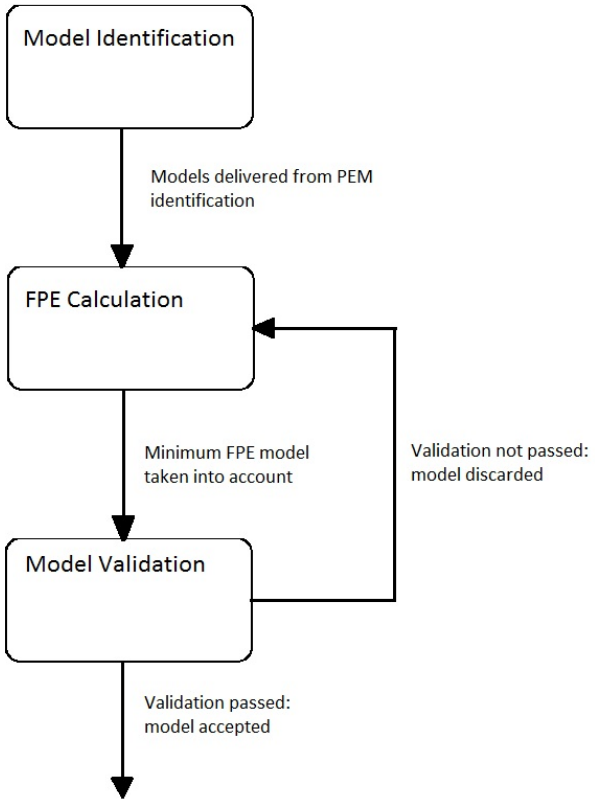

Figure 7.1: Predictive Identification

In the parameters evaluation phase, we verify that the parameters of the candidate model are significantly different from zero. As a rule of thumb, defined with θ_i the $i-th$ parameter of the model and let σ_{θ_i} be the standard deviation

of the uncertainty associated with the parameter θ_i we assume a parameter to be significantly different from 0 if:

$$\left| \frac{\theta_i}{\sigma_{theta_i}} \right| \geq 2 \tag{7.2}$$

If a parameter of higher order is not significant then it can be disregarded, simplifying the model. If a parameter of lower order is not significant then its estimate affects also the higher order parameters that are not reliable anymore. In this case the model is disregarded. Figure 7.2. If a model passes the parameter eval-

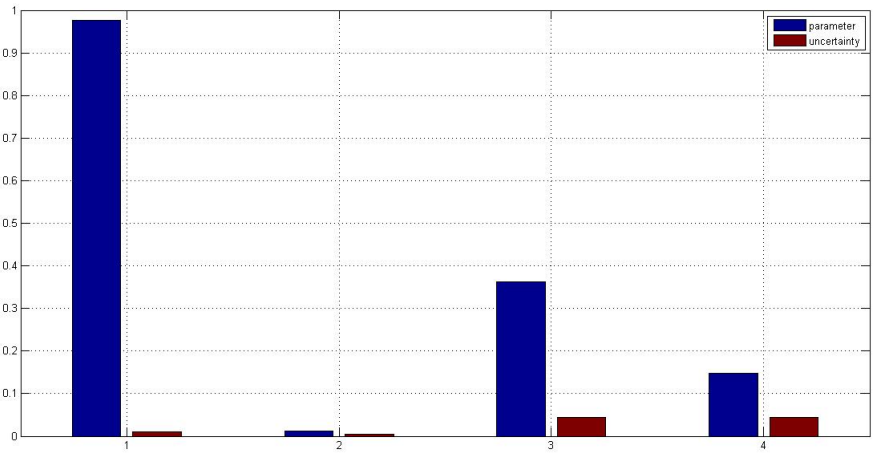

Figure 7.2: Uncertainty affecting the parameters of a model to be tested

uation phase then it is validated through residual analysis. Residual analysis is extremely important: it represents a disturbance input (also referred to as innovation process) that would explain any mismatch between real data and simulated one.If this residual sequence exhibits any trend or structure it would mean that the identification process is not complete and it can be improved. Conversely the model is correct if $\epsilon(t)$-sequence is structureless. In order for the model to pass this test residuals $\epsilon(t)$ should fulfill:

- $\epsilon(t)$ has zero mean and is a white noise: $E[\epsilon(t)\epsilon(t+\tau)] = \lambda^2\delta(t)$;
- $\epsilon(t)$ are independent of the inputs: $E[\epsilon(t)u(t+\tau)] = 0$;
- $\epsilon(t)$ are normally distributed.

The model that first satisfies all the previous tests (lowest FPE, parameter consistency, residuals) is considered the best available. Results obtained from the validation phase show that for some optimal models the poles of $G_t(z)$ and $G_n(z)$

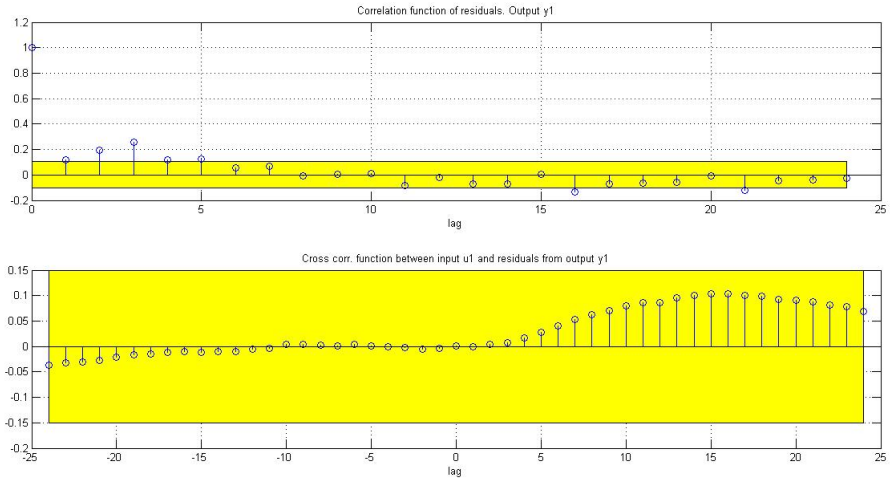

Figure 7.3: Residual test passed by a model

happen almost in the same position. An example is shown in the following models, which represent the systems relating turbine $A02$ to $A03$ calculated referring to samples from 1201 to 1800 (7.3) and 1801 to 2400 (7.4):

$$\begin{aligned} B(z) &= 0.0259z^{-67} \\ C(z) &= 1 + 0.3248z^{-1} \\ D(z) &= 1 - 0.9768z^{-1} \\ F(z) &= 1 - 0.9431z^{-1} \end{aligned} \tag{7.3}$$

$$\begin{aligned} B(z) &= 0.03191z^{-64} \\ C(z) &= 1 + 0.3896z^{-1} \\ D(z) &= 1 - 0.9851z^{-1} \\ F(z) &= 1 - 0.9375z^{-1} \end{aligned} \tag{7.4}$$

This means that the calculated models look like ARMAX models: both the direct part and the noisy part have poles almost in the same position. This fact suggests to repeat the identification-validation procedure with **ARMAX** as target model. The reduction of one degree of freedom in the identification procedure(one polynomial less to calculate for each model) brings the following advantages:

- speeding up the identification-validation phase since there are less models to calculate/validate;

- reduction of the variability of gain and passband of the optimal models calculated for each sequence for each pair of turbine as in: Figure 7.4,Figure 7.5;

- less samples violating the residual test, which means that this model can better explain the underlying reality.

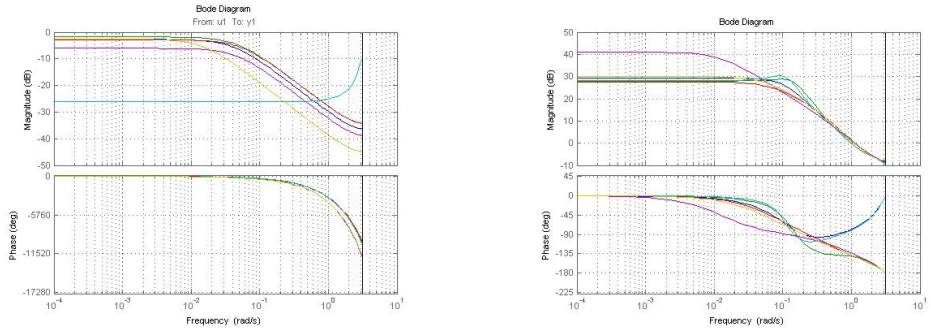

(a) $G_t(z)$ (b) $G_n(z)$

Figure 7.4: Bode plots of $G_t(z)$ and $G_n(z)$

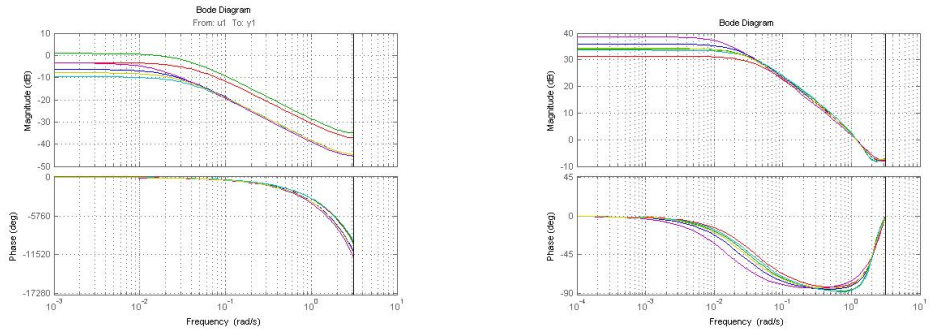

(a) $G_t(z)$ (b) $G_n(z)$

Figure 7.5: Bode plots of $G_t(z)$ and $G_n(z)$

After this second identification-validation phase is performed the models formerly presented to show why ARMAX model are introduced (7.3,7.4) become respectively 7.5,7.6:

$$\begin{aligned} B(z) &= 0.01571z^{-65} \\ C(z) &= 1 + 0.4036z^{-1} \\ A(z) &= 1 - 0.9739z^{-1} \end{aligned} \tag{7.5}$$

$$\begin{aligned} B(z) &= 0.01066 z^{-67} \\ C(z) &= 1 + 0.3248 z^{-1} \\ A(z) &= 1 - 0.9826 z^{-1} \end{aligned} \tag{7.6}$$

A simple inspection on the model structure shows that:

- The bandwidth of the direct contribution $G_t(z)$ is small: $\omega_{G_t(z)} \approx 0.03\text{rad/sec}$ if compared to the total frequency content of the wind; which means that more or less only the instantaneous mean value of the wind travels along the turbines.
- The gain of the direct contribution $G_t(z)$ for each transfer function is around 1, which is reasonable since no big variations in the instantaneous mean value should be expected between 2 points not sufficiently far away.
- The bandwidth of the noisy contribution is wider: $\omega_{G_t(z)} < \omega_{G_n(z)} < \omega_{sampling}$. This confirms the hypothesis of higher order harmonics to fade away during their travel and to be replaced by new uncorrelated eddies.
- The variance of the remote white noise supposed to generate turbulence is low.

From the considerations previously mentioned, it can be derived that there still exist some contributions of the signal that are not explained by the model, in fact the available bandwidth is extended up to $\omega_n < \omega_{sample}$. This is because the underlying reality is time variant and non linear, so mismatches between real world and the models are present.Since the bandwidth of these models is not high enough to explain the wind at frequencies close to the tower natural frequency $\omega_{tow} = 0.24\text{Hz}$ its predictions cannot be used directly to reduce tower vibrations. In Table 7.1 is possible to see a statistic for the identified models both for $G_t(z)$. As previously said, all data available have been divided into subsequences of 600 samples each and for each pair of input-output sequence a model has been identified. This statistic has been built according to the following principle: for each pair of turbine DC-value, poles-zeros position, delay, noise variance have been considered. The numbers appearing in the table are mean-value and variance of the aforementioned values calculated over the models connecting the same pair of turbines but with different input-output sequences.

In order to see if these models are valid either only referring to the pairs of turbines for which they have been calculated or also with other pairs residual analysis has been performed also taking into account sequences belonging to other pairs of turbines: *if model k, being k the input/output subsequences index, has been calculated referring to turbines $A0i$ and $A0i+1$, $i = 1, ..., 7$ then it is tested also on turbines from $A0j+1$ to $A0j+2$, $j = 1, ..., 6$.* This test is necessary in order to find out if the underlying dynamics change from turbine to

turbine or if remains more or less constant. Since residual plots performed in the previously described way behave as if the output error is more or less white (only few samples happen to be outside the $\pm 3\sigma$ confidence interval) we can state that the models identified between one pair of turbine can be used between each pair of turbines in a row starting from $A01$ on. These results are shown in Appendix A and corresponds to residuals produced by the model linking turbines $A03$ and $A04$ when wind sequences belonging to other turbines are taken into account.

7.3 Problem Solution For Spectra Ratio Models

For the models calculated with the ratio of spectra it is not necessary to evaluate the FPE: for each subsequence there exist only one model whose order is already defined. In this phase it is only verified that the residuals are more or less white. Results from the previous validation phase show that optimal models are simple while models calculated with the spectra ratio approach are quite complex (model order ≥ 3). Before going on with the validation phase for spectra ratio models all the identified systems are reduced to the same order of PEM models. To evaluate how much every model can be reduced Hankel singular values have been taken into account: they provide a measurement of the energy for each state in a system, states with relatively small energy can be discarded[2]. After evaluating this quantity the actual simplification can be performed through for example the Matlab function $balred(sys, order)$. Furthermore the reduced models are transformed into discrete time models so that comparisons between the two methods happen in the same domain. Residuals produced are not white. This means that all the calculated models do not capture some important system dynamics. To improve their performances it is possible to use them as starting point for a PEM identification algorithm. Since the first phase of the identification returned models in which the position of poles is deeply different between $G_t(z)$ and $G_n(z)$ parts, the target model in the PEM identification is Box-Jenkins. In this way the estimate is refined through the second phase in which the number of zeros-poles is fixed and the delay is known. What is done in this phase is simply to adjust the position of singularities in the complex plane. After this second

Wind turbine	$E[DC]$	$Var[DC]$	$E[\omega_T]$	$Var[\omega_T]$	$E[\tau]$	$Var[\tau]$
$G_{t_{A0203}}(z)$	0.61	0.08	0.03	7.65e-5	58	30
$G_{t_{A0304}}(z)$	0.55	0.12	0.03	3.86e-5	58	27
$G_{t_{A0405}}(z)$	0.42	0.72	0.04	2.40e-5	60	21
$G_{t_{A0506}}(z)$	0.99	0.09	0.03	6.70e-5	59	29
$G_{t_{A0607}}(z)$	1.13	0.07	0.03	3.90e-5	58	25
$G_{t_{A0708}}(z)$	0.86	0.03	0.03	2.50e-5	59	29

Table 7.1: Model Statistics, $G_t(s)$

step the residual analysis is passed as shown in Figure 7.6.

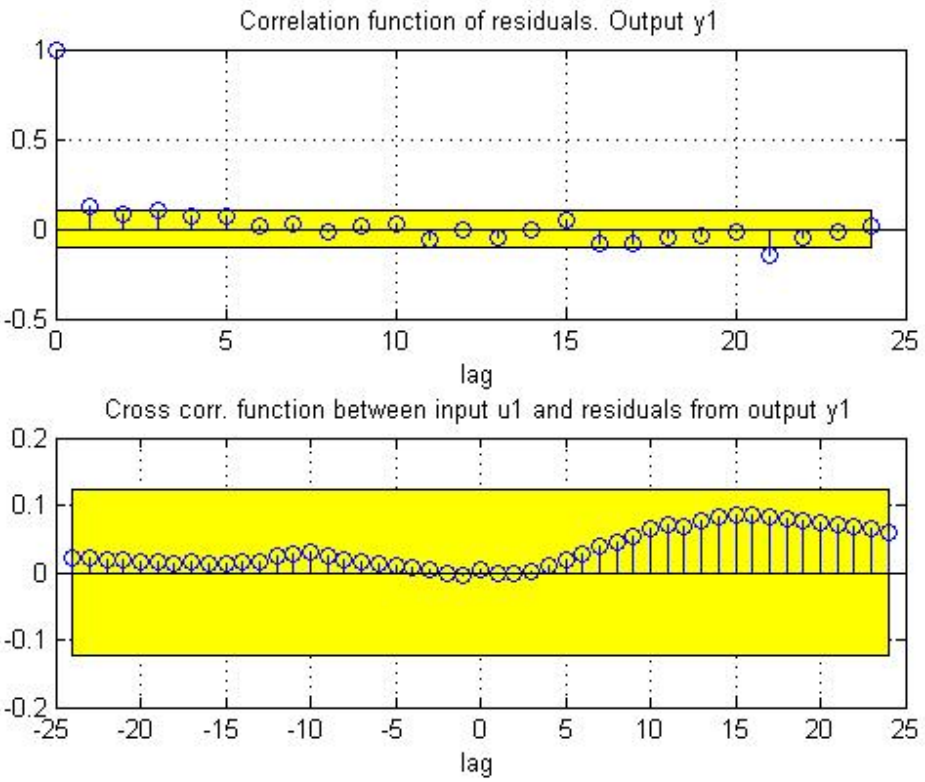

Figure 7.6: A residual analysis plot for a model calculated through SRM

Also in this case it is interesting to see if these models are valid either only referring to the pairs of turbines for which they have been calculated or also with other pairs. Residual analysis has been performed in the same way described for PEM models, that is also taking into account sequences belonging to other pairs of turbines. Also this time only few samples happen to be outside the $\pm 3\sigma$ confidence interval and we can state that the models identified between one pair of turbine can be used between each pair of turbines in a row starting from $A01$ on. These results are shown in Appendix B and corresponds to residuals produced by the model linking turbines $A03$ and $A04$ when wind sequences belonging to other turbines are taken into account.

7.4 Considerations On The Identified Models

As shown, both ways to estimate models relating wind speed between 2 turbines provide consistent models that can be used with more or less good results between each pair of turbines. This means that the wind, traveling, encounters

always the same (or at least similar) transformations: between a pair of turbines only the very low frequency content is preserved and its bandwidth can be fixed at $\omega_{low} = 0.03\text{rad/ sec}$.

7.5 Predictor

Since the models for the process are now available either in ARMAX form or Box-Jenkins, it is possible to calculate the associated predictors. In order to do so, we introduce the following polynomials for Box-Jenkins models:

$$\begin{aligned} \widetilde{A}(z) &= A(z)D(z) \\ \widetilde{B}(z) &= B(z)D(z) \\ \widetilde{C}(z) &= C(z)A(z) \end{aligned} \tag{7.7}$$

so that they are transformed into generalized ARMAX. We can now refer to the correspondent $ARMA$ models, that means disregarding the direct contribution coming from the input. This new models $\widetilde{M}$ should respect the following [19]:

- same degree for numerator and denominator;
- leading coefficient equal to 1;
- no common factors between denominator and numerator;
- zeros and poles inside the unit circle;
- highest grade coefficient equal to 1.

If these hypothesis are verified, then we can calculate the predictor relative to the **ARMA** part, with prediction horizon k, through the long division algorithm and then summing the exogenous input to it. If they are not it is necessary to manipulate the transfer function in order to fulfill all the requests. The ARMA process we start with is in the form:

$$y(t) = \frac{1 + c_1 z^{-1} + c_2 z^{-2}}{1 + a_1 z^{-1}} e(t) = \frac{z^2 + c_1 z + c_2}{z^2 + a_1 z} e(t) = \frac{C(z)}{A(z)} = W(z)e(t) \tag{7.8}$$

The k-step ahead predictor is obtained in 2 steps:

- by mean of long division between numerator and denominator of $W(z)$ it is possible to write $W(z) = \frac{C_k(z)}{A(z)} + Q(z) = W_k(z) + Q(z)$ so that the transfer function is decomposed into its ratio $Q(z)$ plus a residual of the division $W_k(z)$. The subscript k shows that as many division steps must be taken as the prediction horizon.

- The predictor of the output from data is:

$$\hat{y}(t+k|t) = W(z)^{-1}W_k(z)y(t) = \frac{C_k(z)}{C(z)}y(t) \tag{7.9}$$

The coefficients of $Q(z)$ instead are such that, defined the prediction error as:

$$\begin{cases} \epsilon(t) = \hat{y}(t|t-k) - y(t) \\ Var[\epsilon(t)] = (q_0 + q_1 + ... + q_{k-1})\lambda_{n_1}^2 \end{cases} \tag{7.10}$$

The final predictor, which exploits also the direct contribution from $G_t(s)$ is simply obtained by summing the exogenous part previously disregarded.

$$\begin{aligned} &y(t) = a_1 y(t-1) + e(t) + c_1 e(t-1) + c_2 e(t-2) = \\ &A(q)y(t) = C(q)e(t) \end{aligned} \tag{7.11}$$

In order to evaluate the goodness of the predictor we can refer to the following figure of merit:

$$fit\%(k) = (1 - \frac{\|y(t) - \hat{y}(t|t-k)\|}{\|y(t) - \overline{y}\|}) \cdot 100 \tag{7.12}$$

where:

- $y(t)$ is the output EWS sequence;
- $\hat{y}(t|t-k)$ is the output predicted sequence;
- $\overline{y}$ is the mean of $y(t)$;
- k is the prediction horizon.

This figure of merit allow us to evaluate how good is the fit on a scale $\mathcal{R} = [-\infty\%$ - $100\%]$ since the more $\hat{y}(t|t-k)$ is different from $y(t)$ the more $fit\%(k)$ is reduced; $fit\%(k) = 0$ is a special case that happens only when prediction available coincide with the mean value of $y(t)$. In figure Figure 7.7 it is possible to see that, moving forward the prediction horizon, the presence of the direct contribution coming from turbine $i-1$ is beneficial for wind speed predictions at turbine i, while predictions relying only on measurements coming from turbine i tend to approach the aforementioned mean value of wind speed since $fit\%(k) \to 0$ with increasing k.

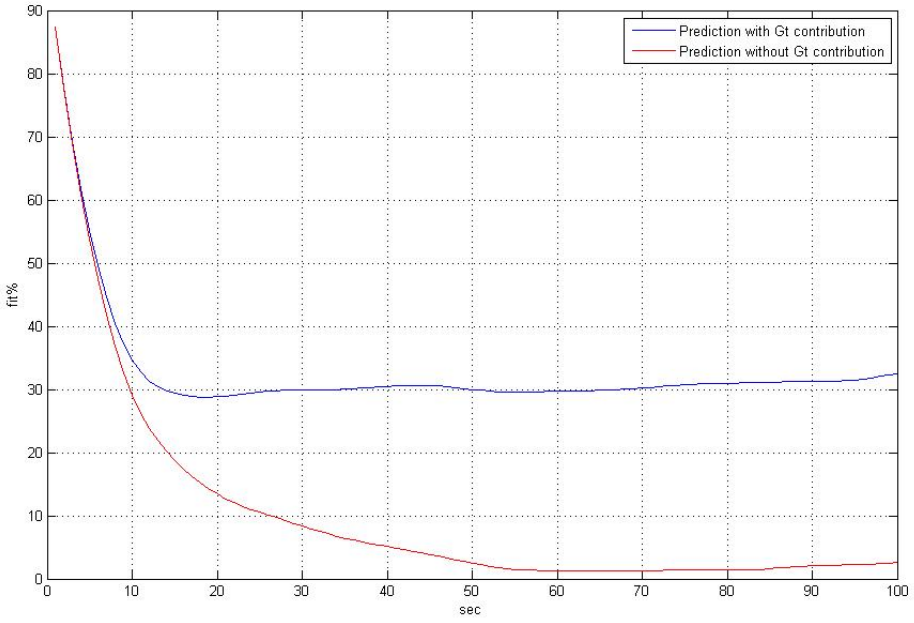

Figure 7.7: $fit\%(k)$ with $G_t(z)$ contribution in blue and without in red.

Chapter 8

Use in Control

A modern wind turbine has different levels of control systems, from top to bottom we can find:

- supervisory control, in which a controller monitors wind resources and the turbine status and determines when it there is enough wind to start up the turbine;
- turbine control that is yaw control which aligns the nacelle to the blowing wind, pitch control that rotates the blades around their axis and is used to control power and tower vibrations and generator control which controls the available torque on the high speed shaft, regulating indirectly the rotor speed.
- actuators and power electronics controllers[14].

A wind turbines has 3 regions of operation which depends on wind speed:

- region 1, that is when a turbine is stopped or is starting up;
- region 2, in which the goal is to capture all the energy available in the wind;
- region 3, in which maximum power available is limited and the goal is to minimize tower vibrations

Normally generator controller and blade pitch controller do not work together: in region 3 produced power is not the maximum available in the wind but is limited while pitch controller acts on β to minimize vibrations, in region 2 pitch angle β is kept constant to a certain value $\overline{\beta}$ and the generator controller tries to set a certain rotor velocity so that $C_p(\overline{\beta}, \frac{\omega_r R_r}{V_e}) = C_{pmax}$. In this work, since wind speed measurements available belong to region 2, we develop a new control system that uses predictions and informations from wind speed in order to better capture energy in the wind. Up to now, with the feedback control system used, the controller could recognize that the turbine was not operating at optimal

speed only when an error occurred, with the control system proposed instead the turbine tries to follow wind speed variations in order to operate always at C_{pmax}. Of course very fast variations cannot be followed because of mechanical limits but produced power increases and, indirectly also vibrations on the tower are minimized.The control law usually proposed for the wind turbine is to let the control torque T_g be given by:

$$\begin{aligned} T_g &= K\omega_r^2 \\ K &= \frac{1}{2}\rho A_r R^3 \frac{C_{p_{max}}}{\lambda_*^3} \end{aligned} \tag{8.1}$$

where K is the gain and λ_* is the tip speed ratio at which $C_{p_{max}}$ occur for a given $\overline{\beta}$. If we assume the turbine to be rigid, as modeled in Chapter 4, we can write:

$$\begin{cases} \dot{\omega}_r = \dfrac{1}{J_{rid}}(T_{aero} - T_g) \\ T_{aero} = \dfrac{1}{2}\rho A_r R \dfrac{C_p(\lambda, \beta)}{\lambda} \\ T_g = K\omega_r \end{cases} \tag{8.2}$$

So considered the system and the control law, the closed loop system looks like:

$$\dot{\omega}_r = \frac{1}{2J_{rid}}\rho A_r R^3 \omega_r^2 \left(\frac{C_p(\lambda, \beta)}{\lambda^3} - \frac{C_{p_{max}}}{\lambda_*^3}\right) \tag{8.3}$$

In this way the system is driven towards $C_{p_{max}}$ so that the maximum power yield is granted. This behavior anyway is achieved only in the ideal case of constant wind speed, if so the system converges to a velocity ω_r that grants maximum power to be produced.

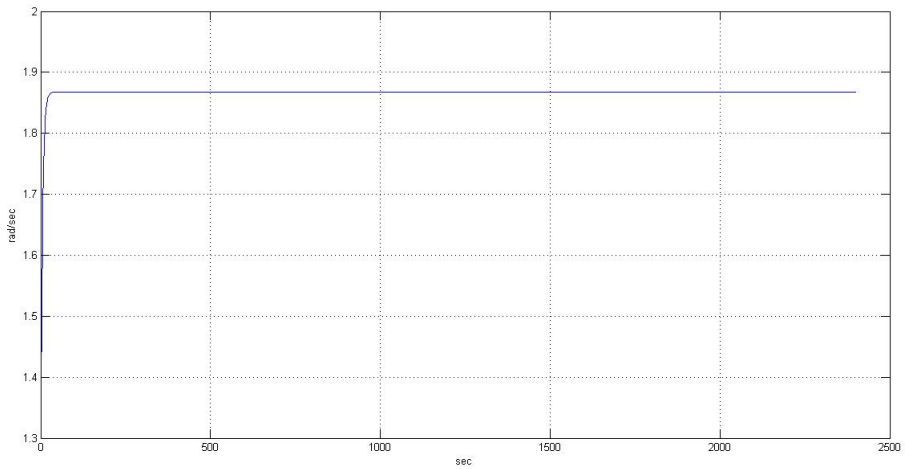

Figure 8.2: Rotor speed approaching a constant value under condition of constant wind speed

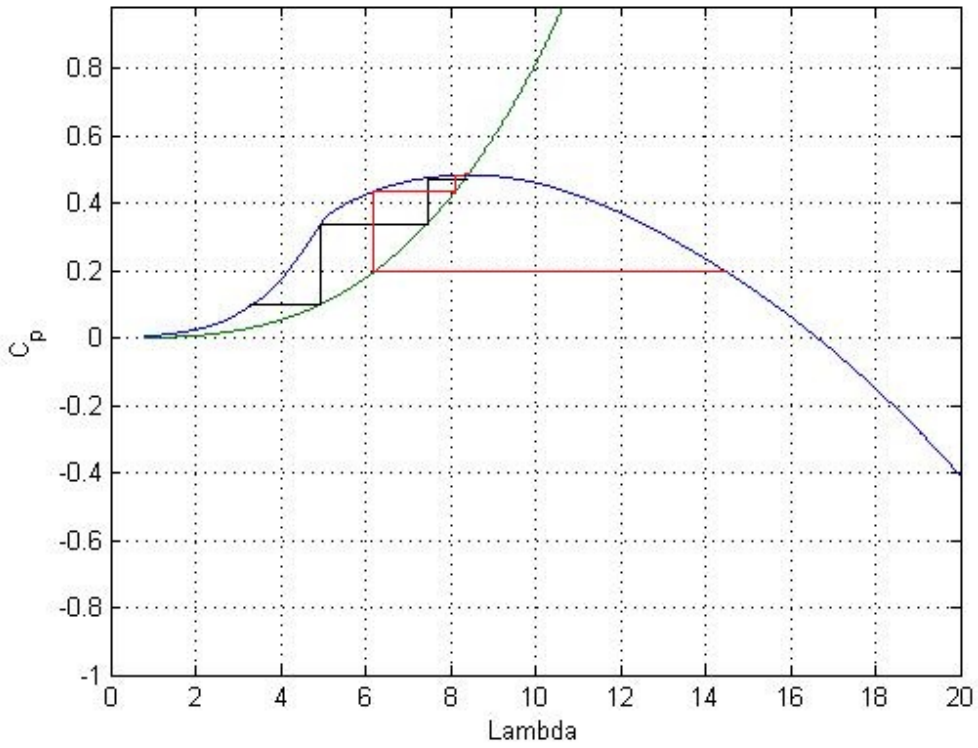

Figure 8.1: Control law driving the system towards $C_{p_{max}}$, in black and red are shown convergences towards $C_{p_{max}}$ from different initial conditions.

In reality the wind is never constant. As previously shown it is characterized by changes on different frequency ranges which affects λ and as a result the turbine is working in a region $[\lambda_{min} - \lambda_{max}]$ and the efficiency is reduced.

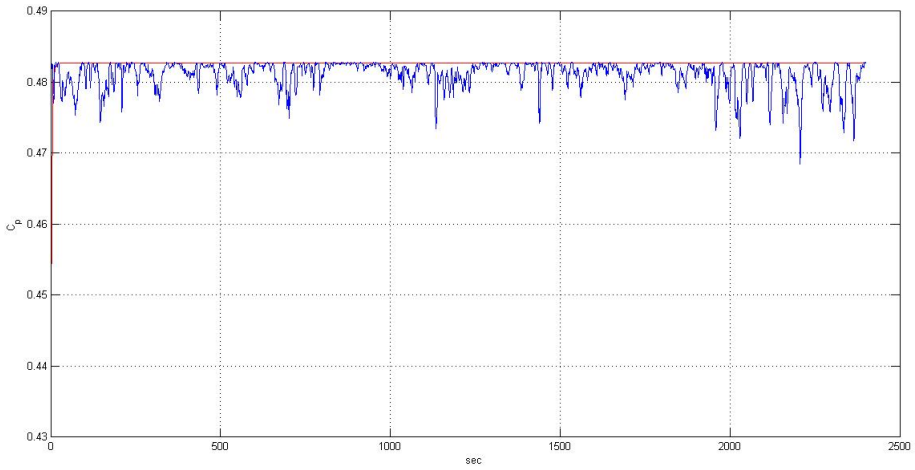

Figure 8.3: Comparison between C_p under constant (ideal) wind in blue and C_p under real wind in red

The new control system proposed consist of a PI controller and a wind predictor that forecasts the turbine velocity reference signal to be followed. In order to do so, since in region 2 pitch angle is kept constant it is possible to write:

$$C_p(\lambda, \beta) = C_p(\lambda, \overline{\beta}) = C_p(\lambda) \tag{8.4}$$

λ_* at which C_p has its maximum is known so, by inverting the simple relationship of λ with respect to ω_r and exploiting wind predictions it is possible to compute the optimal rotor velocity reference:

$$\begin{cases} K_{pred} = \dfrac{\lambda_*}{R_r} \\ \hat{\omega}_r(t+k|t) = K_{pred}\hat{V}_e(t+k|t) \end{cases} \tag{8.5}$$

With this approach T_{aero} is considered to be a disturbance while the input (control) signal remains the generator torque. Since our goal is to control the rotor velocity, the PI controller is designed to control the rigid drive-train previously described. The control technique followed consists in imposing phase margin and bandpass for the closed loop system. This methodology has been chosen since the system turbine is affected by uncertainties and variabilities in the parameters so a high enough phase margin is required. As regards the bandpass it is necessary to guarantee that the closed loop system will be able to follow the wind up to a

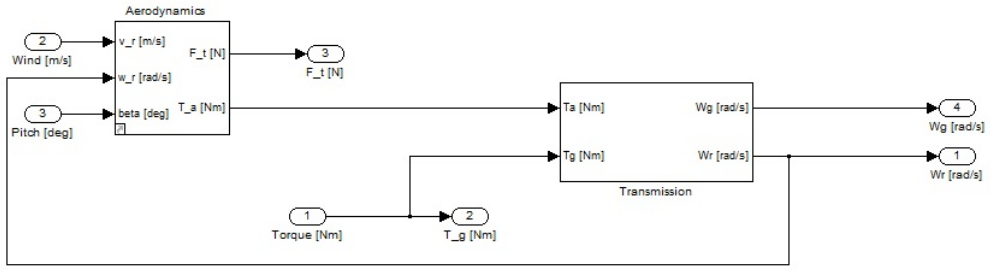

Figure 8.4: Model of the transmission adopted in control

frequency where its contribution is important. Spectral analysis of EWS shows that above $\omega_{wind} = 0.32\text{rad/sec}$ the information contained in the wind is very small. Being the controller, in continuous time, the following:

$$PI(s) = K_p \frac{1 + sT_i}{sT_i} \tag{8.6}$$

and being $L(s)$ the loop transfer function:

$$L(s) = PI(s)G_{drive-train}(s) \tag{8.7}$$

we choose for the closed loop system

$$F(s) = \frac{L(s)}{1 + L(s)} \tag{8.8}$$

a cut-off frequency $\omega_c = 0.6\text{rad/sec}$ and a phase margin $\phi_m = 60\,\text{deg}$ because of the previous considerations. It is possible to find the correct value for the parameter solving the following equation to find T_i:

$$\phi_m = 180 - 90 + \arctan \omega_c T_i - \arctan \omega_c T_p \tag{8.9}$$

while K_p is found through:

$$|L(j\omega_c)| = 1 \tag{8.10}$$

The closed loop system looks like: Results are shown in the following figures. It can be seen that this system grants the turbine to work closer to $C_{p_{max}}$, so the produced power is increased. A second benefit due to this other control system

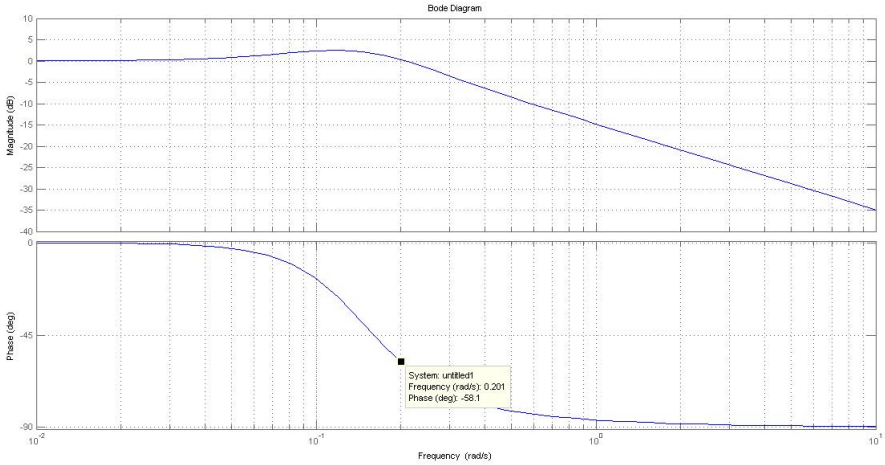

Figure 8.5: Bode diagram of the closed loop system

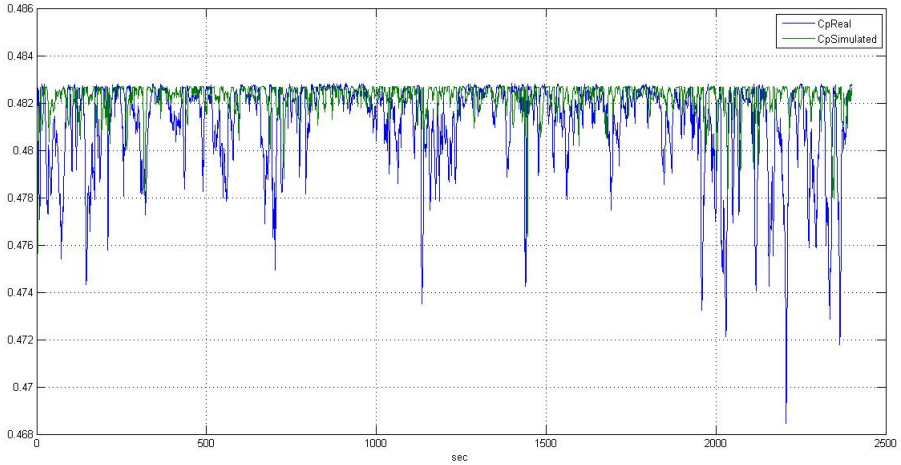

Figure 8.6: Coefficient C_p, real in blue and simulated in green

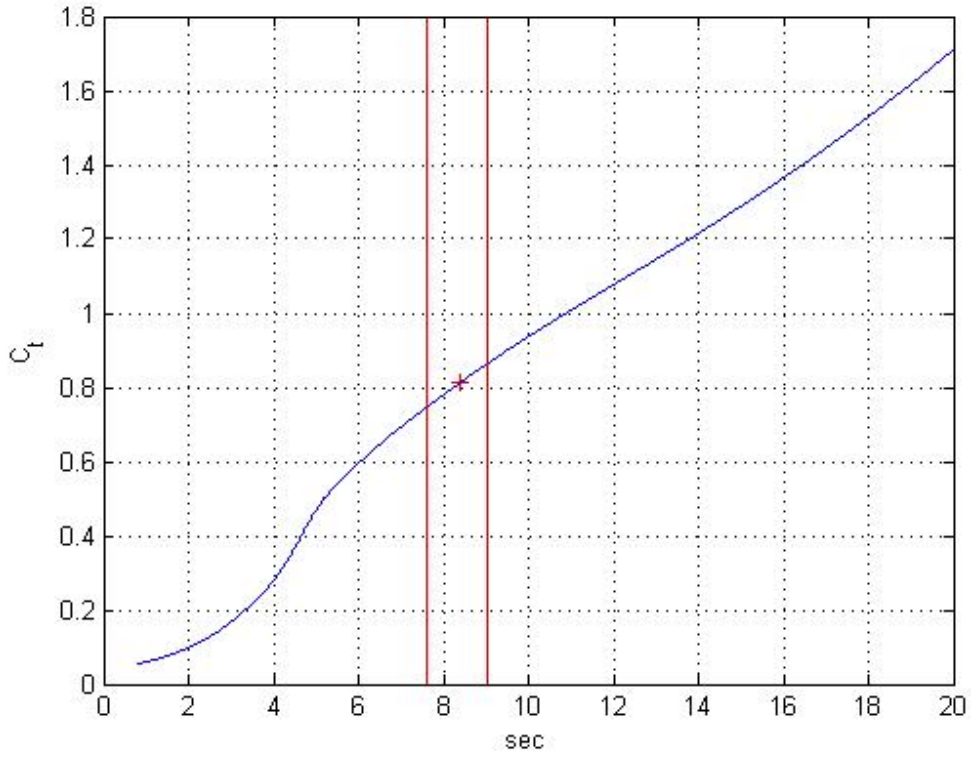

Figure 8.7: Coefficient C_t for a given β

is that the force acting on the tower is reduced, since less variations of λ implies less variation of the coefficient C_t through which the aerodynamic force depends: $F_{aero} = \frac{1}{2}\rho A_r C_t(\lambda, \beta) V_e^2$. A drawback instead is the higher control torque needed in order to follow fast wind speed variations with the rotor.

Chapter 9

Conclusions and Future Developments

The purpose of this work was to look for the existence of a mathematical model that could explain how wind is transformed along its way in a wind-farm because of interactions between turbines.

In order to do this we introduced a fake measurement for the wind, called *Effective Wind Speed*, that is more reliable than the anemometer measurement. The proof for this, as shown, is that the power that would be produced if the wind was EWS is much more similar to the real produced one rather than using NWS.

This measurement was used to identify input output ARMAX models, based on 600 samples each for identification. What can be seen by looking at these models is that their characteristics change over time even though they more or less have the same shape. This fact can be explained with the following:

- EWS can be expressed as $EWS(t) = v_m(t) + v_t(t)$;
- $\exists \mathcal{S} : \dot{x} = f(x, u)$ so that $EWS_{i+1} = \mathcal{S}(EWS_i)$ and in general is non linear;
- $v_m(t)$ vary slowly and polarizes the system in different working regions: $\overline{\mathcal{S}} \to 0 = f(x, v_m)$;
- what is identified is $\delta\mathcal{S}$, such that $\mathcal{S} = \overline{\mathcal{S}} + \delta\mathcal{S}$;
- because of the aforementioned slow variations in wind speed $\delta\mathcal{S}$ varies over time.

A new control model has been proposed: in order to better track wind variations the rotor velocity set point is forecast from wind speed predictions. It has been shown that even with a very simple controller like a PI performances (from the point of view of produced power and tower vibrations) are enhanced. On the

other hand in order to better track the wind a higher torque is required.

Since it has been shown that a simple mathematical model that explains transformation between one turbine to the other exists, future work in this direction should be in the direction of adapting slowly the identified system and the predictor to slow variations in the parameters.

A more refined way to identify the delay is needed, since its correct estimate will affect all the future estimation work.

A more refined control technique which involves predictions should be investigated in order to better exploit the information available; in addition also the best prediction horizon should be found in order to fully exploit the information available.

Data available for this analysis were limited to 8 turbines in a column. Having a wider spread of data, coming from different columns and/or directions, other behaviors such as interactions among rows could be evaluated. It could also have been possible to construct a greater statistic and work out a better interaction model among turbines and a better control system that exploits data predictions coming from several turbines.

Chapter 10

Appendix A

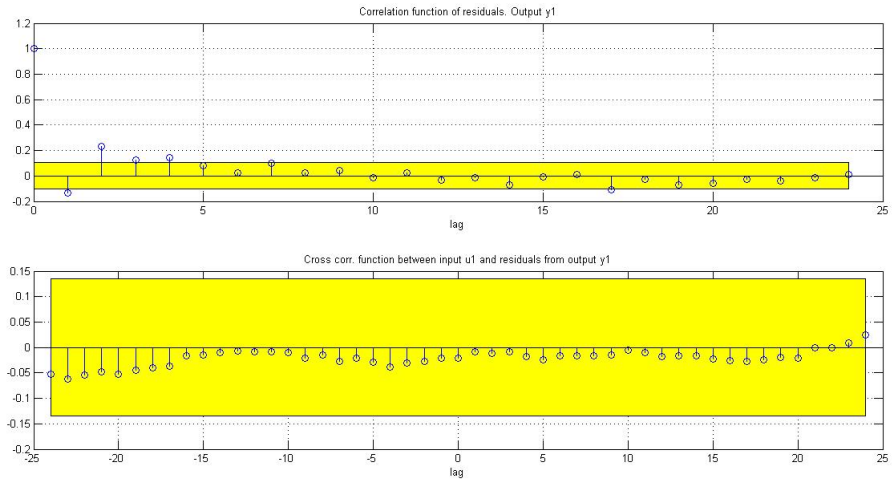

Figure 10.1: Residual analysis plot produced by model linking turbines $A03$ - $A04$ evaluated on sequence acting on turbine $A01$ - $A02$

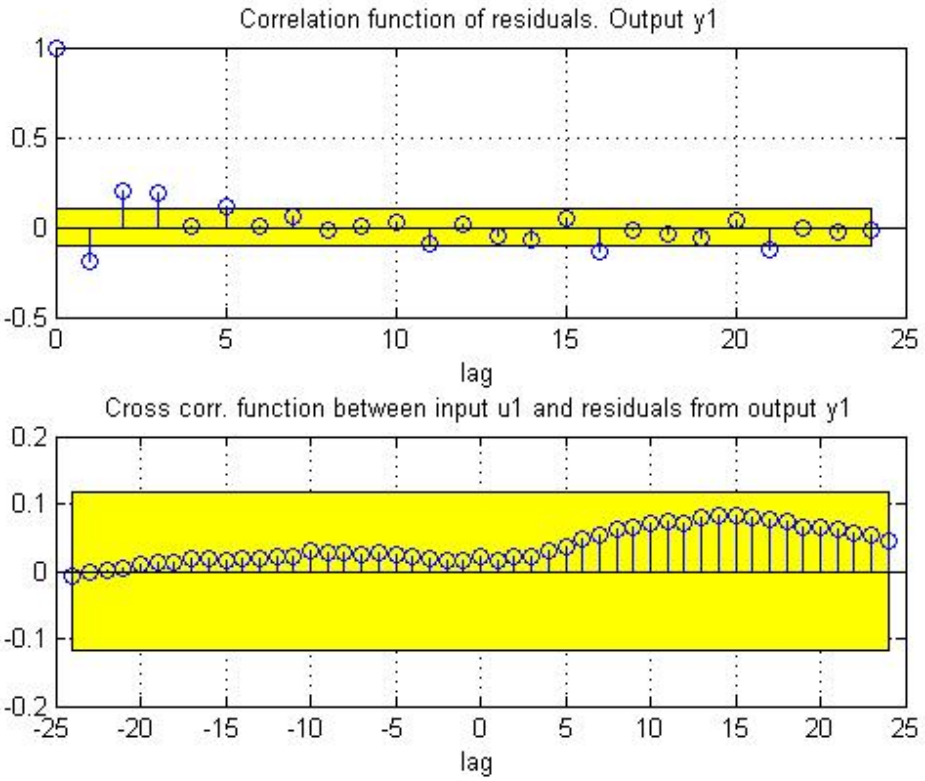

Figure 10.2: Residual analysis plot produced by model linking turbines $A03$ - $A04$ evaluated on sequence acting on turbine $A02$ - $A03$

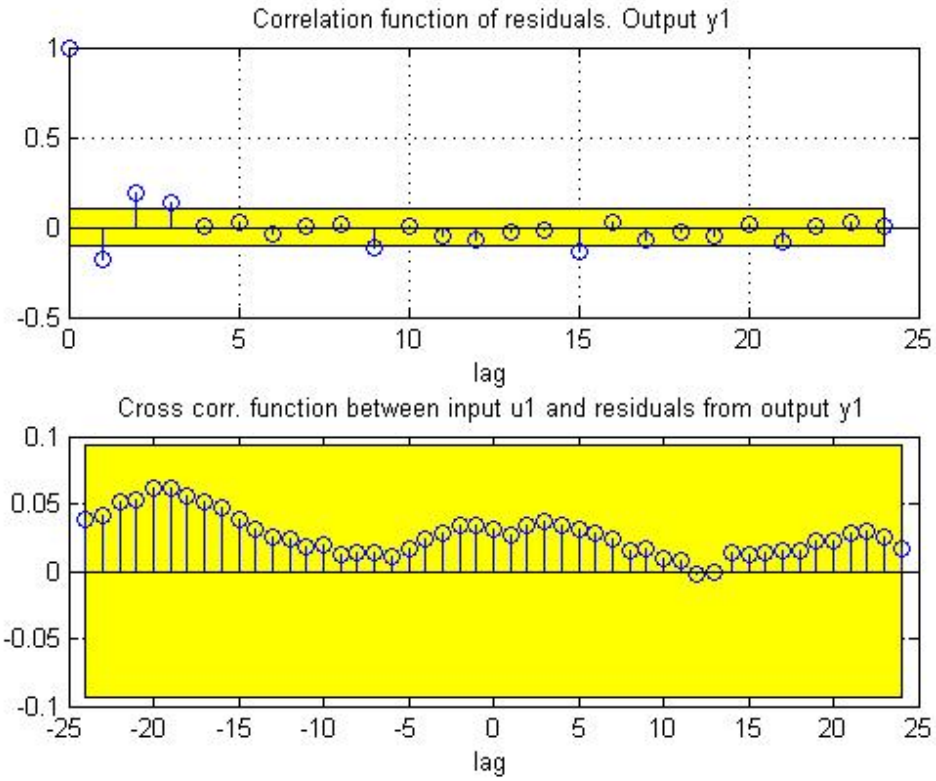

Figure 10.3: Residual analysis plot produced by model linking turbines $A03$ - $A04$ evaluated on sequence acting on turbine $A04$ - $A05$

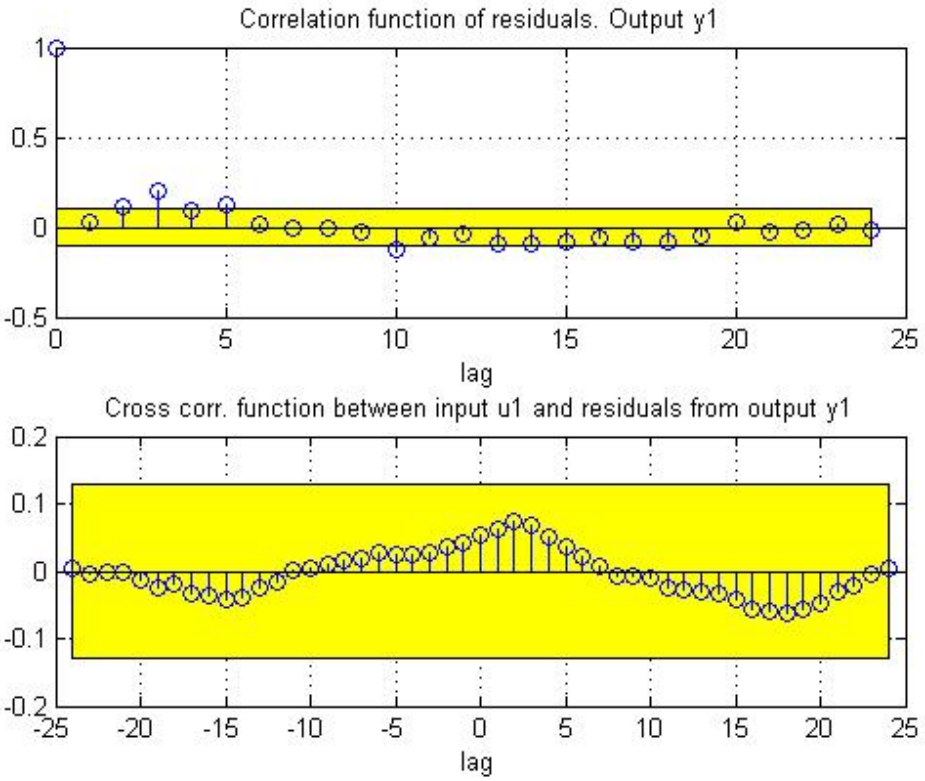

Figure 10.4: Residual analysis plot produced by model linking turbines $A03$ - $A04$ evaluated on sequence acting on turbine $A05$ - $A06$

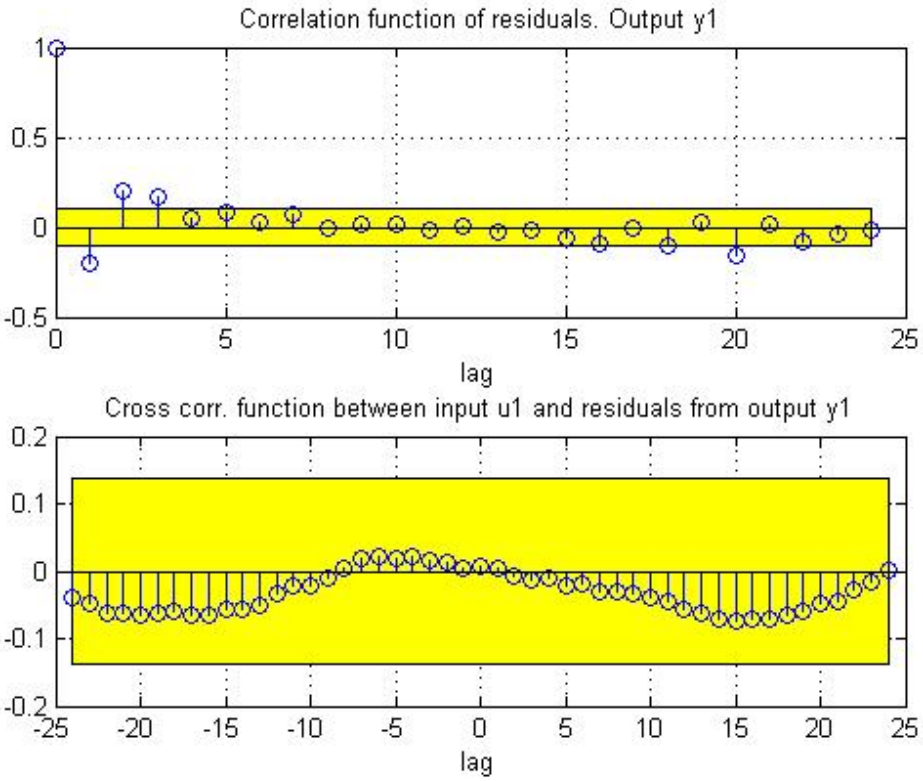

Figure 10.5: Residual analysis plot produced by model linking turbines $A03$ - $A04$ evaluated on sequence acting on turbine $A06$ - $A07$

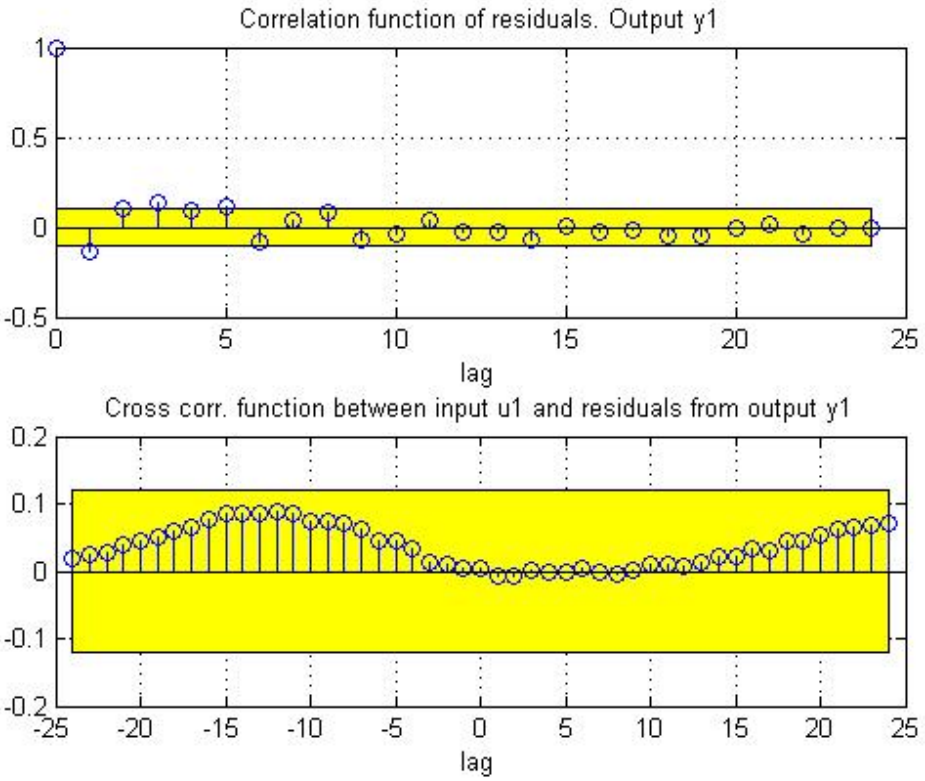

Figure 10.6: Residual analysis plot produced by model linking turbines $A03$ - $A04$ evaluated on sequence acting on turbine $A07$ - $A08$

Chapter 11

Appendix B

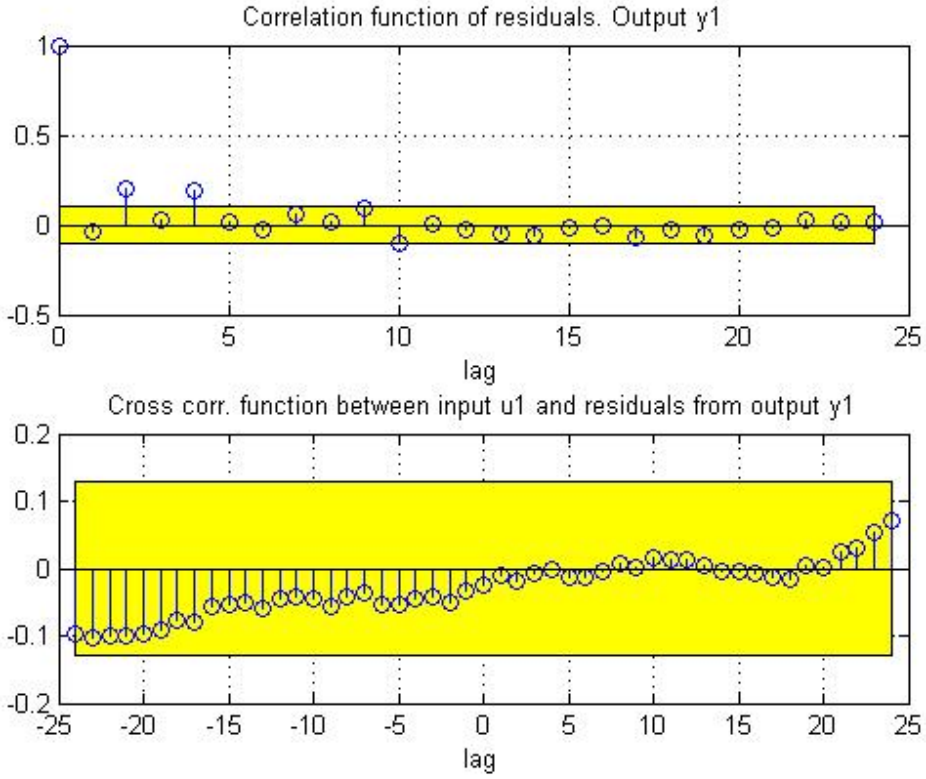

Figure 11.1: Residual analysis plot produced by model linking turbines $A03$ - $A04$ evaluated on sequence acting on turbine $A01$ - $A02$

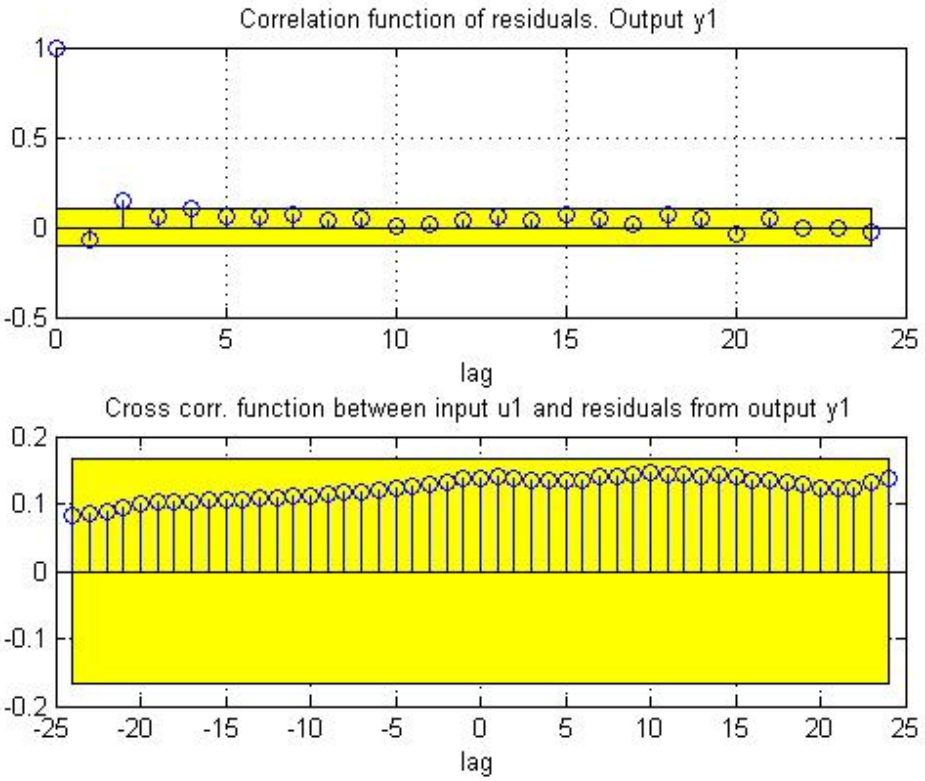

Figure 11.2: Residual analysis plot produced by model linking turbines $A03$ - $A04$ evaluated on sequence acting on turbine $A02$ - $A03$

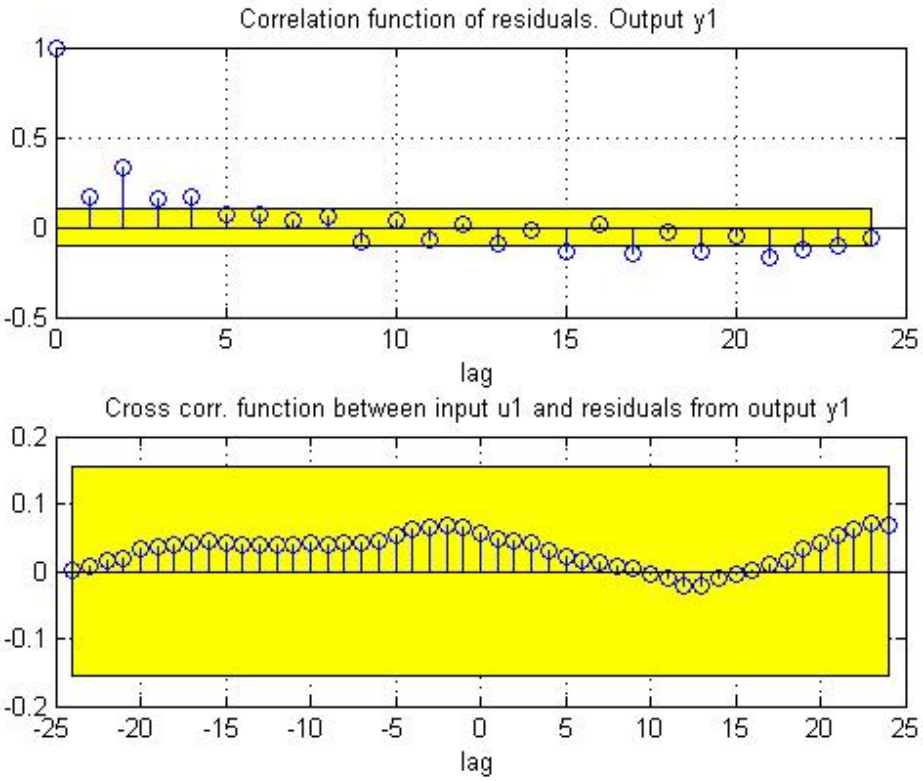

Figure 11.3: Residual analysis plot produced by model linking turbines $A03$ - $A04$ evaluated on sequence acting on turbine $A04$ - $A05$

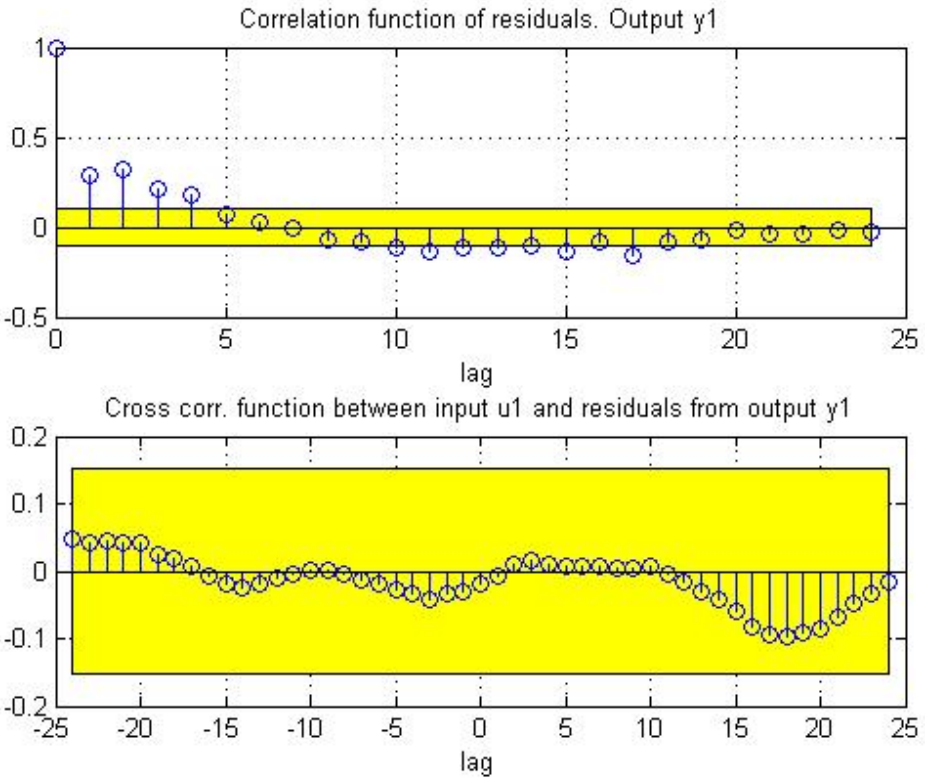

Figure 11.4: Residual analysis plot produced by model linking turbines $A03$ - $A04$ evaluated on sequence acting on turbine $A05$ - $A06$

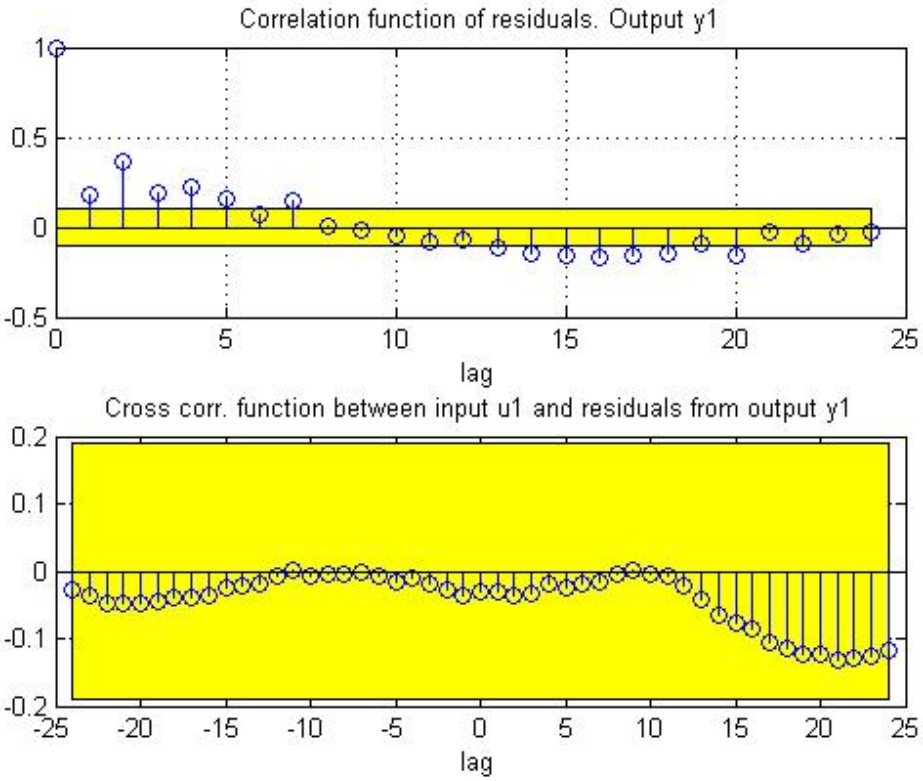

Figure 11.5: Residual analysis plot produced by model linking turbines $A03$ - $A04$ evaluated on sequence acting on turbine $A06$ - $A07$

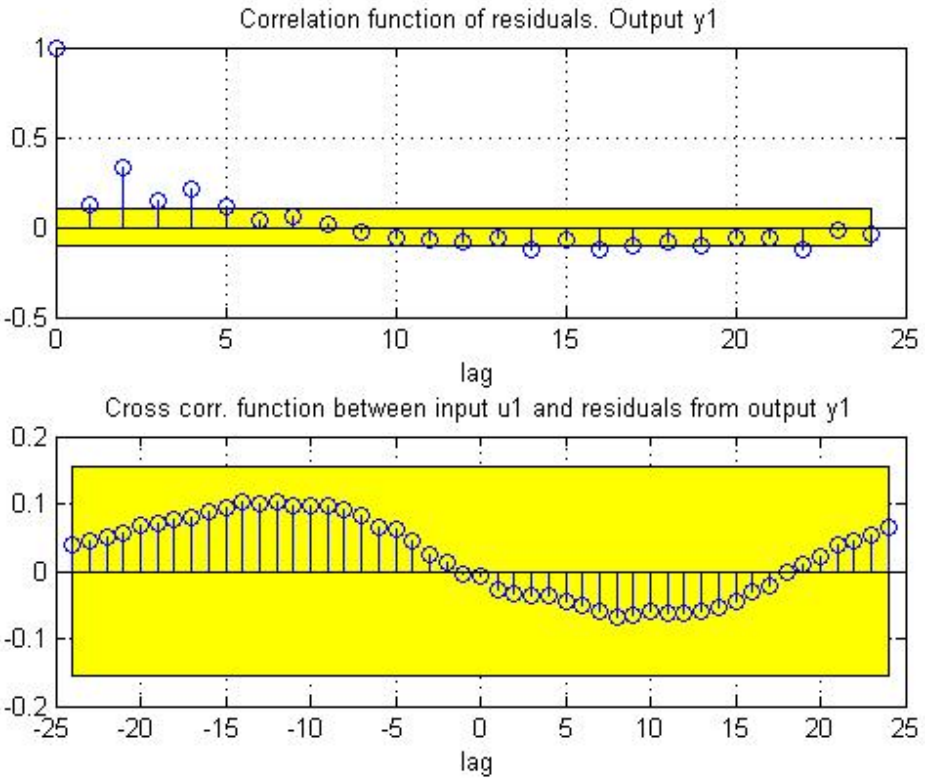

Figure 11.6: Residual analysis plot produced by model linking turbines $A03$ - $A04$ evaluated on sequence acting on turbine $A07$ - $A08$

Bibliography

[1] http://www.awea.org/pubs/documents/outlook

[2] http:/www.en.wikipedia.org.

[3] http://www.srh.noaa.gov/jetstream/synoptic/wind.htm.

[4] Matlab user's guide.

[5] Moskalenko N. Rudion K. Orths A. Study of wake effects for offshore wind farm planning. *Modern Electric Power Systems*, 2010.

[6] Grewal MS. Andrews AP. *Kalman Filtering 2nd edition*. Prentice Hall, 2001.

[7] Sharpe D. Burton T. Jenkins N. Bossanyi E. *Wind Energy Handbook*. Wiley, 2001.

[8] SÃ¸rensen et al. Operation and control of large wind turbines and wind farms. *Technical Report RisÃ¸-R-1532(EN)*, 2004.

[9] Alexiadis M. Dokopoulos P. Sahsamanoglou H. Wind speed and power forecasting based on spatial correlation models.

[10] Alexiadis M. Dokopoulos P. Sahsamanoglou H. Manousaridis I. Short term forecasting of wind speed and related electrical power.

[11] Pao L. Johnson K. A t utorial on the dynamics and control of wind t urbines and wind farms.

[12] Brown L. Wind electric generation soaring.

[13] Manwell J. F. McGowman J. G. Rogers A. L. *Wind Energy Explained, Theory, Design and Application*. John Wiley and Sons Ltd, 2002.

[14] Johnson K.E. Pao Y.L. Balas M.J. Fingersh L.J. Control of variable-speed wind turbines. *IEEE Control Systems Magazine*, June 2006.

[15] Knudsen T. Bak T. Soltani M. Prediction models for wind speed at turbine locations in a wind farm. *Wiley Online Library*, August 2011.

[16] Nielsen HA. Madsen H. SÃ¸rensen P. Ultrashort term wind speed forecasting. *European Wind Energy Conference Exhibition*, November 2004.

[17] Johansson R. *System Modeling and Identification.*

[18] Bittanti S. *Identificazione dei Modelli e Sistemi Adattativi.* Pitagora Editrice Bologna, 2004.

[19] Bittanti S. *Teoria della Predizione e del Filtraggio.* Pitagora Editrice Bologna, 2004.